Chain formation and glial tube assembly in the shift from neonatal to adult subventricular zone of rodent forebrain

Chain Formation and Glial Tube Assembly in the Shift from Neonatal to Adult Subventricular Zone of the Rodent Forebrain

PAOLO PERETTO, [1] CLAUDIO GIACHINO, [1] PATRIZIA AIMAR, [2] ALDO FASOLO, [1,3]AND LUCA BONFANTI[2,3] *

[1] Department of Animal and Human Biology, University of Turin, 10153 Turin, Italy
[2] Department of Veterinary Morphophysiology, University of Turin, 10095 Grugliasco, Italy
[3] Rita Levi Montalcini Center for Brain Repair, University of Turin, 10153 Turin, Italy

ABSTRACT

The subventricular zone (SVZ) is regarded as an embryonic germinal layer persisting at the end of cerebral cortex neurogenesis and capable of generating neuronal precursors throughout life. The two distinct compartments of the adult rodent forebrain SVZ, astrocytic glial tubes and chains of migrating cells, are not distinguishable in the embryonic and early postnatal counterpart. In this study we analyzed the SVZ of mice and rats around birth and throughout different postnatal stages, describing molecular and morphological changes which lead to the typical structural arrangement of adult SVZ. In both species studied, most changes occurred during the first month of life, the transition being slightly delayed in mice, in spite of their earlier development. Important modifications affected the glial cells, eventually leading to glial tube assembly. These changes involved an overall reorganization of glial processes and their mutual relationships, as well as gliogenesis occurring within the SVZ which gives rise to glial cell subpopulations. The neuroblast cell population remained qualitatively quite homogeneous throughout all the stages investigated, changes being restricted to the relationships among cells and consequent formation of chains at about the third postnatal week. Electron microscopy showed that chain formation is not directly linked to glial tube assembly, generally preceding the occurrence of complete glial ensheathment. Moreover, chain and glial tube formation is asymmetric in the medial/lateral aspect of the SVZ, being inversely related. The attainment of an adult SVZ compartmentalization, on the other hand, seems linked to the pattern of expression of adhesion and extracellular matrix molecules.

Indexing terms: development; neurogenesis; migration; astrocyte; neural stem cell

The adult forebrain subventricular zone (SVZ; also referred to as subependymal layer; Boulder Committee, 1970) is a remnant of the primitive germinal layers providing neurogenesis throughout life. The SVZ is unique among adult neurogenetic sites, since newly generated neuronal precursors undergo long distance migration to finally differentiate into the olfactory bulb (Altman, 1969; Lois and Alvarez-Buylla, 1994; Lois et al., 1996). Although the SVZ is commonly considered an area of the adult brain fully retaining embryonic features, substantial differences do exist in the morphological and molecular composition of its perinatal and adult counterpart. For instance, the prenatal and early postnatal SVZ contains an open olfactory ventricle which closes after birth in rodents, giving rise to SVZ rostral extension (RE) or rostral migratory stream (RMS). The most striking differences concern two aspects;

Grant sponsor: Ministero dell'Istruzione, dell'Università (Fondo per l'Incentivazione della Ricerca di Base); Grant number: RBNE01YRA3;
Grant sponsor: Regione Piemonte; Grant number: 1837/27;
Grant sponsor: University of Turin, Compagnia di San Paolo.
*Correspondence to: Luca Bonfanti, Department of Veterinary Morphophysiology, Via Leonardo da Vinci, 44, 10095–Grugliasco, Turin, Italy.
E-mail: luca.bonfanti@unito.it

1) types and spatial distribution of glial cell populations, and 2) different modes of cell migration, at varying developmental stages.

Radial glia is the most abundant glial cell type in embryonic SVZ (Misson et al., 1991; Rakic, 2003), replaced in the adult by a special type of protoplasmic astrocyte arranged to form longitudinally oriented channels, called glial tubes (Lois et al., 1996; Jankovski and Sotelo, 1996; Doetsch et al., 1997; Peretto et al., 1997). Recent studies have suggested that adult SVZ astrocytes derive directly from embryonic radial glia (Gaiano et al., 2000; Alves et al., 2002; Tramontin et al., 2003). Accordingly, embryonic radial glial cells have been recognized as being capable of generating both astrocytic and neuronal precursors (Malatesta et al., 2000; Noctor et al., 2001) before undergoing their transformation into mature astrocytes (Misson et al., 1991). Consequently, the current hypothesis is that astrocytes in the adult SVZ could act as slow-dividing neural stem cells, capable of generating the progeny of neuronal precursors migrating to the olfactory bulb (Doetsch et al., 1999; Laywell et al., 2000; Tramontin et al., 2003). Nonetheless, the recent findings increase the number of interpretations for SVZ astrocytes, now including 1) a guide in cell migration; 2) a substrate in cell migration; 3) a boundary between tissue compartments; 4) stem cell function; and 5) stem cell niche, thus making it more complex to sharply define a role for glia in the SVZ (see Jankovski and Sotelo, 1996; Tramontin et al., 2003; Peretto et al., 1999, 2004).

Another major issue concerns the arrangement of migrating cells throughout postnatal development as well as their relationship with changing glial structures. Despite changes in types and orientation of glial cells, a tangential migration of neuronal precursors constantly takes place in the SVZ from embryonic/perinatal periods (Luskin, 1993; Pencea and Luskin, 2003; Law et al., 1999) to adulthood (Lois and Alvarez-Buylla, 1994). At birth, cells migrate orthogonally to the radial glia processes (Kishi, 1990; Luskin, 1993; Goldman and Luskin, 1998), whereas in the adult a characteristic “chain” migration involving bulks of cells sliding into the longitudinally oriented glial tubes has been described (Lois et al., 1996; Jankovski and Sotelo, 1996; Peretto et al., 1997). A recent study has described prenatal development of RMS (Pencea and Luskin, 2003), whereas others have focused on radial glia/ astrocyte transformation (Alves et al., 2002; Tramontin et al., 2003) and cell proliferation/differentiation in the ventricular zone at a cellular level (Tramontin et al., 2003).

In the present study we addressed overall modifications occurring in the SVZ of rats and mice at late embryonic/ postnatal stages, showing that major changes leading to the assembly of the “adult” SVZ do occur during the first three postnatal weeks. In particular, attention has been focused on: 1) assembly of astrocytic glial tubes from embryonic/early postnatal radial glia; 2) mutual contact among migrating cells, leading to the formation of characteristic “chains,” and their relationships with the glial compartment and surrounding environment; and 3) molecular changes affecting overall SVZ set up and its cell populations, as well as modifications in the surrounding forebrain tissue. In order to link morphological modifications leading to glial tube assembly and chain formation with changes in the molecular pattern of cells and matrix we used electron microscopy, light microscopy, and immunocytochemistry for antigens expressed by mature andimmature glial cells. Moreover, the distribution of three molecules linked respectively to cell migration (PSA-NCAM), assembly of the astrocytic meshwork (Cx43), and a boundary effect in the extracellular matrix (tenascin-C) was studied. Our results will be discussed taking into account recent findings from other laboratories.

MATERIALS AND METHODS

Tissue preparation

Brains were obtained from 30 young (embryonic (E)18, postnatal (P)0, P3, P6, P9, P13, P17, P21, P25, P30; three animals for each age) and three adult (3–5 months old) Wistar rats (Charles River, Italy), and 36 young (E18, P0, P3, P6, P9, P13, P15, P17, P21, P25, P45, three animals for each

age) and three adult (3 months old) CD-1 mice (Charles River, Italy) for light microscopic studies. An additional nine (P6, P13, P21) young rats and mice were used for electron microscopy. All experiments were performed in accord with current Italian law, under authorization of the Italian Ministry of Health (n. 66/99-A). For light microscopy, animals were deeply anesthetized with intraperitoneal ketamine (Ketavet, Gellini, Italy) and xilazine (Rompun, Bayer, Germany), then perfused intracardially first with a heparinized saline solution (25 IU/ml in 0.9% NaCl, over 1–3 min) followed by a freshly prepared solution of 4% paraformaldehyde in 0.1 M sodium phosphate buffer, pH 7.4. After dissection, brains were post-fixed overnight in the same fixative, then cut with a vibratome in 75 μm-thick slices or cryoprotected in ascending sucrose solutions, frozen in liquid nitrogen-cooled isopentane at –70°C, and cryostat sectioned in series (20 m). Coronal and parasagittal sections were processed for immunocytochemistry, respectively, as free- floating sections or onto TESPA-coated slides. For electron microscopy, animals were perfused with 2% glutaraldehyde + 1% paraformaldehyde and 0.2% picric acid in 0.1 M sodium phosphate buffer, pH 7.4. Brains were postfixed in the same fixative for 2 hours, then coronal vibratome sections (200 μm) were cut at the level of the horizontal arm of the rostral extension (RE), and fixed in osmium-ferrocyanide for 1 hour at 4°C. They were then stained en bloc with 1% uranyl acetate in maleate buffer, pH 5.3, for 1 hour at 4°C, ethanol-dehydrated, and embedded in Araldite, as previously described (Peretto et al., 1997). Ultrathin sections were examined with a Philips CM10 transmission electron microscope.

5-Bromo-2'-deoxyuridine (BrdUrd) injections

Mice received intraperitoneal single injections of BrdUrd (Sigma, St. Louis, MO; 8 mg/100 g body weight) dissolved in 0.1 M Tris. Six animals were killed 2 hours postinjection (P3, P90). Another eight animals were killed 3, 22, or 40 days after the treatment (P6, P25, P45).

Immunohistochemistry

Immunohistochemical reactions were carried out using single peroxidase and double immunofluorescence methods on cryostat sections incubated overnight at 4°C with a single primary antibody or a combination of primary antibodies and 1% normal serum of the same donor species of the secondary antiserum. For double staining a combination of two indirect immunofluorescence procedures with FITC + Cy3-conjugated antibodies were used. The following primary antisera and antibodies were used: 1) anti- PSA-NCAM, diluted 1/3,000 (monoclonal IgM to α-2,8- PSA residues of polysialic acid; G. Rougon, Marseille, France); 2) anti-BrdUrd, 1/1,000 (rat monoclonal, Harlan, Indianapolis, IN); 3) anti-Ki67 1:2,000 (Novocastra, UK); 4) anti-class III β-tubulin, 1/600 (TU-J1, monoclonal and polyclonal, BAbCO, Richmond, CA); 5) anti-glial fibrillary acidic protein, 1/1,000 (GFAP, polyclonal, Dako, Carpinteria, CA); 6) anti-s100b 1/15,000 (polyclonal, SwantBellinzona, Switzerland); 7) anti-vimentin, 1/800 (monoclonal, Dako); 8) anti-tenascin-C 1/1,000 (rat-monoclonal, Sigma); 9) anti-nestin, 1/10 (mouse-monoclonal, Hybridoma Bank, University of Iowa, USA); 10) anti-connexin 43, 1/100 (Cx-43, polyclonal, R. Bruzzone, Heidelberg, Germany); 11) anti-brain lipid binding protein 1/1500 (BLBP, polyclonal, T. Anthony, Rockefeller University, New York); 12) anti-aldolase C/zebrin II 1/100 (ALDC/ZII monoclonal, R. Hawkes, University of Calgary, Canada); 13) anti-NeuN 1:800 (Chemicon, Temecula, CA). All the antibodies were diluted in a solution of 0.01 M PBS, pH 7.4, containing 0.5% Triton X-100. Antimouse and antirabbit Cy3 conjugated antibodies (1:800, Jackson ImmunoResearch, West Grove, PA), affinity-purified antirat (mouse adsorbed), antimouse, or antirabbit biotinylated antibodies (1:250, Vector, Burlingame, CA) followed by avidin Cy3 (1:800, Jackson ImmunoResearch) or avidin FITC (1:400, Vector) served as immunolabels. When two polyclonal primary antibodies were used (BLBP-S100β), staining of the first antigen–antibody complex was

performed with antirabbit Cy3 secondary Ab. This step was followed by a blocking reaction with an antirabbit Fab fragment (80 ng/ml; Jackson ImmunoResearch) (Giacobini et al., 2004) for 1 hour at room temperature followed by PBS washes, fixation (4% formalin, 30 minutes), and washes (PBS) before application of the second primary Ab, which was visualized with biotinylated antirabbit antibody followed by avidin FITC.
Sections were mounted in a solution of 1,4- diazabicyclo[2.2.2]octane (Dabco, Sigma) and observed with a conventional epifluorescence and with a laser scanning confocal system using appropriate filters.
For immunogold labeling, ultrathin sections collected on nickel grids (200 mesh) were treated for 5 minutes with a saturated aqueous solution of sodium metaperiodate, rinsed in 1% Triton X-100 in Tris-buffered saline (TBS- Triton) 0.5 M, pH 7.4, and incubated for 1 hour in 10% normal serum. Grids were then placed overnight at room temperature on drops of primary anti-GFAP antibody (polyclonal, Dako, 1:100). After extensive rinsing in 1% bovine serum albumin in TBS (TBS-BSA) they were incubated in the appropriate gold-conjugated secondary antibody (20 nm, 1:15) for 1 hour at 37°C, rinsed again in TBS-BSA, transferred into drops of 2.5% glutaraldehyde in phosphate buffer 0.1 M, pH 7.4, and finally washed in distilled water. The sections were then counterstained with uranyl acetate and lead citrate before observation with the electron microscope.

Cell counting

The counts of cell types (%) identified by electron microscopy were performed on ultrathin coronal sections cut at the level of the horizontal arm of the SVZ rostral extension, obtained from 6-, 13-, and 21-day-old animals (n = 6). Low-magnification micrographs were taken along the two axes of the SVZ-RE area. All nucleated cells showing features of neuroblasts, mature astrocytes, immature glial cells, ependymal cells, microglia, and mitotic and apoptotic features (total = 6,197 cells) were counted.

Preparation of figures

Light photomicrographs were digitized using a Phase One PowerPhase digital camera (Phase One, Denmark) fitted to a Leica DMRX microscope (Leica Microsystems, Deerfield, IL). Analysis and digital photography of the double immunofluorescence was carried out using a laser- scanning Olympus Fluoview confocal system (Olympus Italia, Milano). Black and white negatives from Philips CM10 electron microscope were imported into PhotoShop using an Epson Perfection (3200 Photo) scanner. Digital images were brightness, color, and contrast balanced, assembled into montages using PhotoShop 5.5 (San Jose, CA). Plates of photomicrographs were printed using a Fuji Fujix Pictrography 3000 printer (Fuji Photofilm USA, Carlstadt, NJ).

RESULTS

By using cresyl violet staining and conventional histology on forebrain sections, the SVZ was clearly distinguishable at all the postnatal stages examined as a relatively compact mass of small, tightly packed cells (Figs. 1, 2A– C). As previously described (Altman, 1969; Smart, 1961), its diameter was different in relation to the anterior/ posterior levels examined and the age of the animals, being proportionally more enlarged at the early postnatal stages (from about 300 μm at birth to about 100 μm in the adult mouse). Up to P0 –3 (mouse) or P3– 4 (rat) the olfactory ventricle was still abundantly present along the central axis of the olfactory bulb (Figs. 1A, 3). Starting from these stages, the anterior horn of the lateral ventricle was replaced by the RE, which thus loses its contact with ventricular cavities; only occasionally were some clusters of residual ependymal cells observed at different levels of the RE, as described in the adult RMS of rats (see also Peretto et al., 1999). All the observations were carried out in the SVZ-RE since here the adult

glial tubes and chains run parallel to each other, thus allowing a better identification of the two compartments (chains of neuroblasts and astrocytic glial tubes). We know from a recent study (Gritti et al., 2002) that stem cells reside both in the ventricular part of the SVZ and in the RMS, the latter being not simply a migratory pathway. Cell types were identified using light microscopic immunocytochemistry with glial, neuronal, and cell proliferation markers, from birth to adulthood. An ultrastructural analysis was carried out at P6, P13, and P21 stages to better characterize cell types, their distribution, and mutual relationships during the establishment of the SVZ compartmentalization. Particular attention was focused on the interface between SVZ-RE and surrounding parenchyma, referred to as the RE outer limit (RE-OL). Such a limit was generally well recognizable with all the above-mentioned techniques. Nevertheless, it appeared sharper along its medial side, whereas it was less identifiable on the lateral side, in contact with the white matter of the lateral olfactory tract.

Due to similar results obtained in rats and mice, a qualitative description will be given for both species, referring to each of them only when remarkable differences were observed. As to minor ifferences restricted to the temporal pattern, these are summarized in Tables 1– 4.

Glial cell compartment: spatial arrangement and molecular characterization

Different glial antigens yielded complementary information about the overall distribution of glial cells throughout postnatal development of the SVZ. Antibodies raised against the cytoskeletal proteins vimentin, nestin, and GFAP were useful in studying the complexity of glial processes (Fig. 1; Table 1). Vimentin and nestin, although downregulated during nervous tissue maturation (Shaw et al., 1981; Pixley and De Vellis, 1984), do persist in the adult SVZ, associated with glial tube astrocytes (Peretto et al., 1997, 1999; Doetsch et al., 1997), thus allowing the visualization of most glial cells in adult neurogenic areas from embryogenesis to adulthood. The immunoreactivity for GFAP was considered only when clearly detectable glial processes were observed; in the SVZ this occurred starting from P9 (rats) and P13 (mice), being very faint at P6 (Fig. 1; Tables 1, 4). In particular conditions, depending on antibody sources, fixation procedures, or the species studied, GFAP immunostaining could be detected earlier and in different cell populations (see e.g., Shu et al., 2003; Alves et al., 2002). Other markers, such as S-100b, BLBP (see Hartfuss et al., 2001), and to a lesser extent ALDC/ ZII, allowed a better visualization of glial cell bodies (Fig. 2). Radial glia being the prevalent glial cell population in the perinatal and early postnatal stages, its overall distribution has been studied using immunocytochemistry for vimentin (in rats), nestin, BLBP (Feng and Heintz, 1995), and ALDC/ZII (Staugaitis et al., 2001) (Figs. 1, 2; Table 1). In addition to cryostat sections, thick vibratome slices treated immunocytochemically for vimentin and nestin were used to provide an overall visualization of the remarkable extension of the radial glia processes in postnatal animals, from P0 onward (Fig. 3). The occurrence of glial cell subpopulations and their topographical localization in the SVZ have been studied using anti-BLBP, -ALDC/ZII, -S100β, -GFAP antibodies and a combination of them (Figs. 1, 2).

At E18 (not shown) and around birth (P0 –1) radial glial cells were predominant throughout the forebrain. In the SVZ-RE and olfactory bulb, vimentin-positive radial glia processes originating from cell bodies located in the olfactory ventricle wall and frequently organized to form small fascicles were observed to span radially the SVZ-RE as well as the surrounding tissue, with slight changes at the RE-OL level (Fig. 1A). Numerous cell bodies, revealed with anti-BLBP and -ALDC/ZII antibodies, were already present throughout the SVZ-RE area, with a slight prevalence in the medial part.

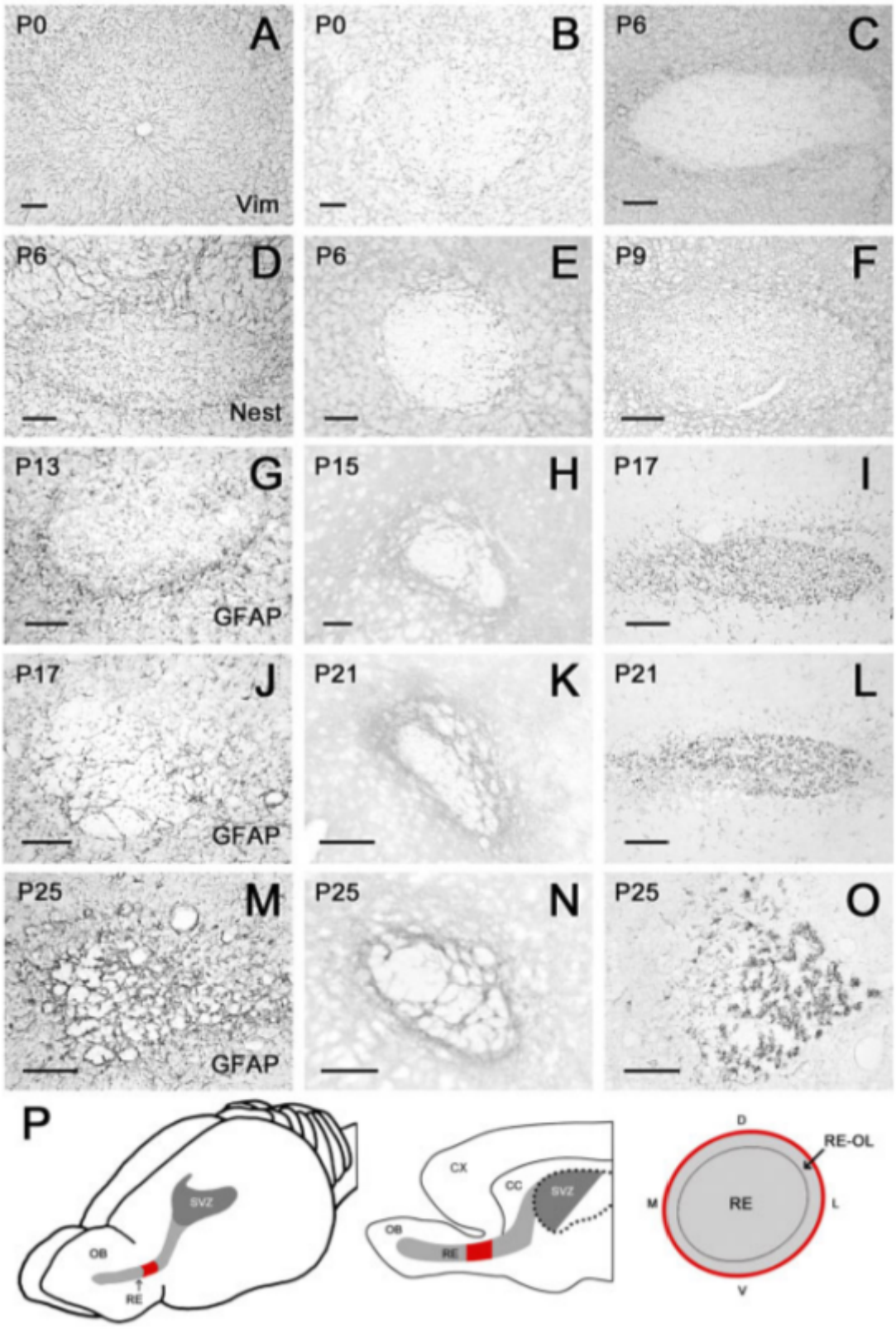

Fig. 1. Distribution of glial cells and their processes (visualized with different glia-related antigens, left column), tenascin-C (middle), and PSA-NCAM (right column) immunoreactivities in the postnatal rodent SVZ-RE at different postnatal stages. Vimentin and nestin identify glial cells in the early postnatal period, whereas GFAP as a marker of the whole astrocytic network is more useful later. Some antigens in the same line are shown at different ages, choosing the stages in which changes were more evident. Note that, starting from the third postnatal week, glial structures are more organized on the medial side (left) of the SVZ, whereas the compartmentalization of the SVZ-RE by tenascin-C (H,K,N) and the assembly of PSA-NCAM+ chains (I,L,O) are more evident on the lateral side (right). The slant of the SVZ-RE main axis in coronal section is different in mice and rats. In the photographs referring to the rat, it has been

turned clockwise to become horizontal. P, Schematic representation of the area examined. All images presented in this study were obtained from the same portion (here indicated in red) of the horizontal arm of the SVZ rostral extension (RE, light gray), shown in a three-dimensional view (left), sagittal view (middle), and coronal view (right; restricted to the RE). SVZ, subventricular zone (dark gray). The dotted line (middle) marks the lateral ventricle. OB, olfactory bulb; CX, cortex; CC, corpus callosum; RE-OL, outer limit of the rostral extension; M, medial; L, lateral; D, dorsal; V, ventral. The location of all images is indicated in each figure legend. Scale bars = 50 μm.

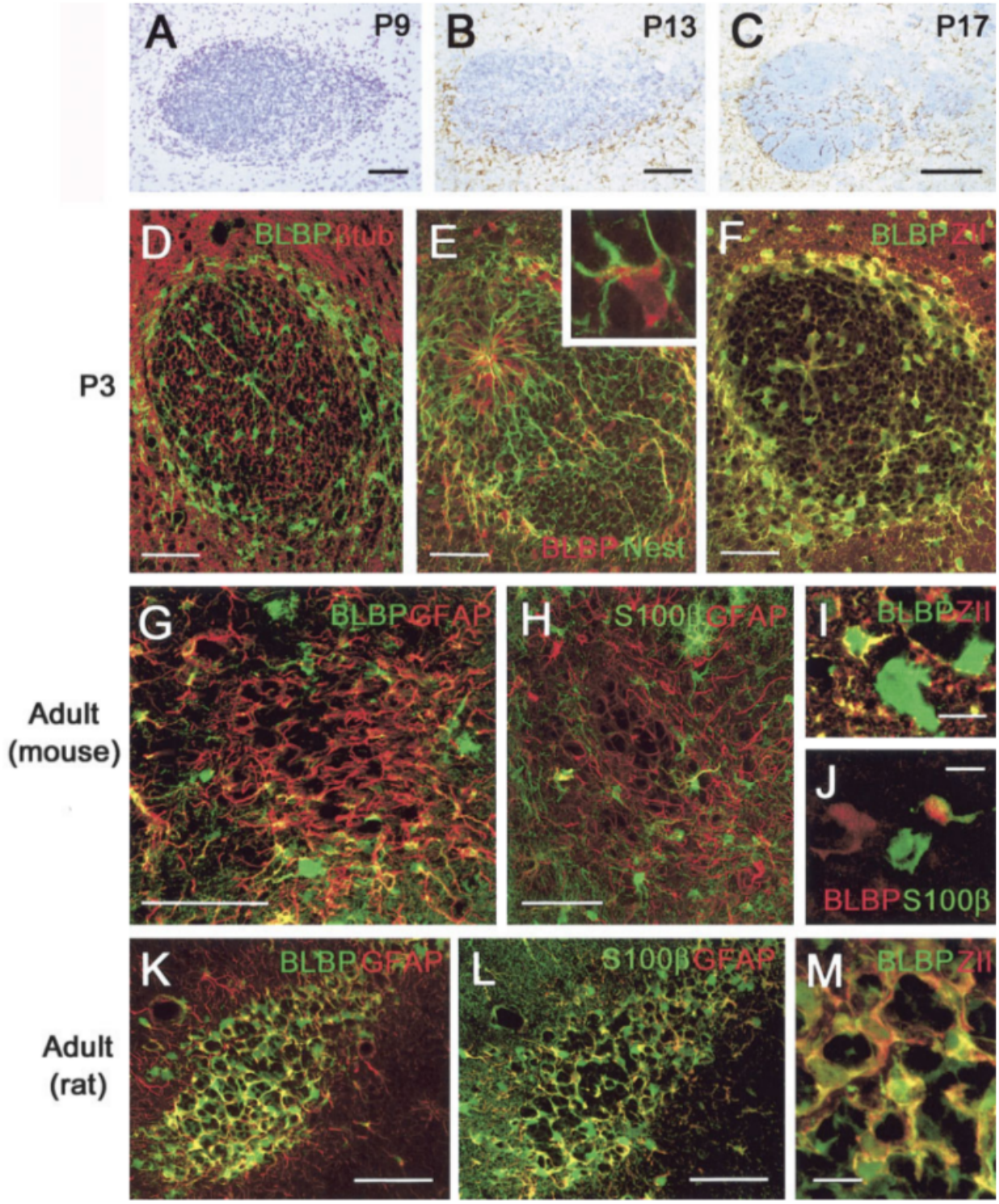

Fig. 2. Molecular characterization and occurrence of antigenically different cell subpopulations in the SVZ-RE at different postnatal stages. Cresylviolet stainings (A–C) identify the mass of SVZ cells and its topographical overlapping with glial modifications (B,C; GFAP staining, brown). BLBP, nestin, and ALDC/ZII allow a complete visualization of glial cells in early postnatal periods (D–F). Cell bodies are better detectable with BLBP and ALDC/ZII, whereas nestin

marks cell processes. At later stages, small glial cell subpopulations containing BLBP (G,I) and S100β (H,J) are detectable in mice (G–J) but not in rats (K,M). Scale bars = 50 μm in A–H, K,L; 10 μm in I,J,M.

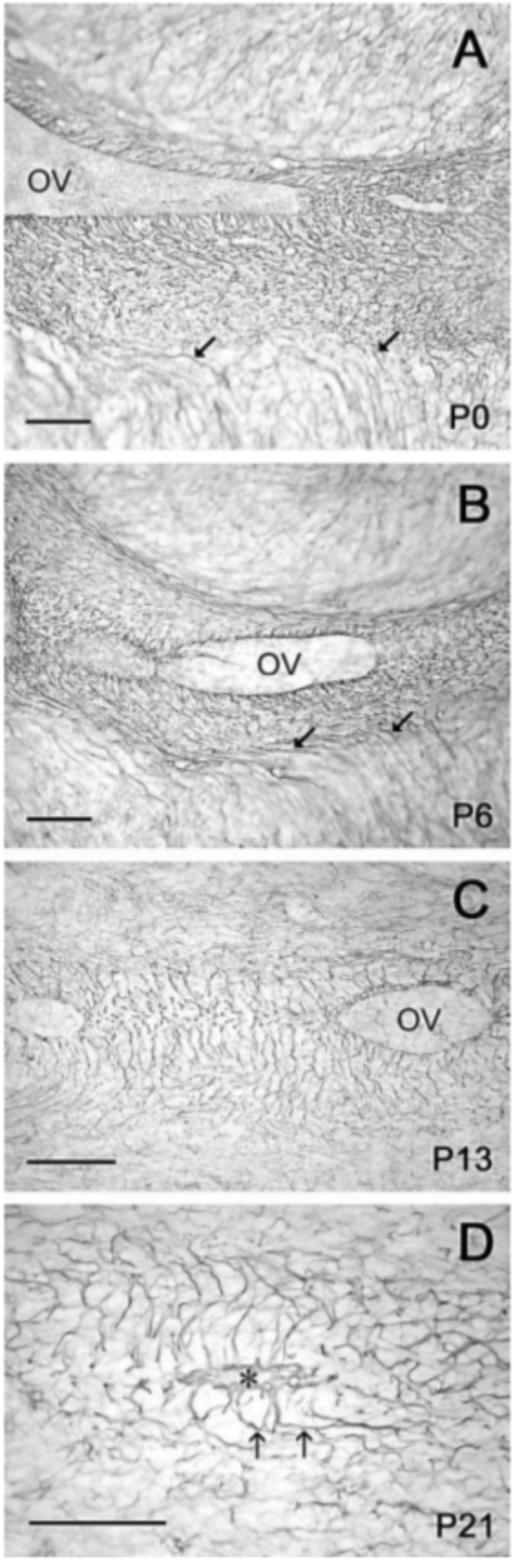

Fig. 3. Visualization of glial cells and processes in sagittal, thick vibratome sections of the rat SVZ-RE, treated with anti-vimentin antibody. Note the progressive closure of the olfactory ventricle (OV), the fine meshwork of glial processes within the SVZ-RE, and the change in direction (from radial to tangential, then becoming radial again) of radial glia processes at the interface between the SVZ-RE and the surrounding tissue (A,B, arrows). Radial glia-shaped cells are still present at P21 in the core of the SVZ-RE, associated with residual ependyma (asterisk). Their processes are mainly oriented tangentially (D, arrows). Scale bars = 100 μm.

TABLE 1. Morphological and Molecular Changes Observed in Glial Cells of the Postnatal SVZ

	Overall morphology	NEST	VIM	GFAP	BLBP	ALDC/ ZII	S100β	
							R	M
E18	radial glia	+++	+++	−	+++	+++	+++	+
P0	fine network of radial glia/astrocytic processes	+++	+++	−	+++	+++	+++	+
P3		+++	+++	−	+++	+++	+++	+
P6	fine network of radial glia/astrocytic processes (denser at the RE-OL)	+++	+++	+	+++	+++	+++	+
P9		+++	+++	++	+++	+++	+++	+
P13	more evident aggregation of astrocytic processes	+++	+++	++++ (M)	+++	+++	+++	+
P17	astrocytic network with septa	+++	+++	+++	+++	+++	+++	+
P21	glial tube outline	++	++	++++	+++	+++	+++	+
P25/30	glial tubes	+	++	++++	+++++ (M)	+++	+++	+
Adult		+	++	++++	++++ (M)	+++++ (M)	+++	+

(R) rat; (M) mouse; ++++, for GFAP indicates more tightly packed processes, not an increase in the number of cells.

TABLE 2. Morphological and Molecular Changes Observed in Migrating Cells of the Postnatal SVZ

	Organization	Clefts	Cytology	β-Tub
P0	homogeneous mass	No	Migrating neuroblasts (Lois	+++
P3	large masses	No	et al., 1996; Doetsch et	+++
P6	large masses and chains	yes	al., 1997; Jankovski and	+++
P13	small masses and chains		Sotelo, 1996; Peretto et	+++
P17	chains		al., 1997)	+++
P21				+++
P25				+++
P30				+++

TABLE 3. Ultrastructural Features of the Postnatal SVZ; Occurrence of Morphologically Different Cell Types (%)

	Features	P6	P13	P21
Neuroblasts (type A cells)	Small size, dark cytoplasm	92.43	91.14	88.63
Astrocytes (type B cells)	Watery cytoplasm	0.84	2.47	7.77
Immature glial cells*	Large/intermediate size, cytology intermediate between type A and B	6.49	4.84	2.45
Mitotic figures		0.24	0.11	0.26
Apoptotic figures		0	0.10	0.07
Microglia		0	1.34	0.82

*Immature glial cells consist of radial glia-like cells (at P6), immature astrocytes, and C-like cells (at P13–P21).

Starting from P3, and more evidently at P6, in coronal views radially oriented glial processes were restricted to the area immediately adjacent to the olfactory ventricle wall and to the tissue surrounding the SVZ-RE, whereas most of the SVZ-RE itself was filled with a great number of glial processes forming a small-mesh net (Fig. 1). Cresylviolet counterstainings as well as β-tubulin stainings clearly showed that the area occupied by this glial net was exactly overlapping with the mass of tightly packed, migrating neuroblasts of the RMS (Fig. 2). In BLBP and ALDC/ZII stainings a great number of glial cell bodies were detectable through the entire SVZ-RE thickness, indicating that many of them had already retracted from the ependymal layer. A great number of these cell bodies were grouped along the RE-OL (Fig. 2). At P6, an increase was observed in the density of vimentin/nestin-positive glial processes along the RE-OL (Fig. 1), and the BLBP and ALDC/ZII stainings confirmed the accumulation of most glial cell bodies at the peripheral level (Fig. 2). Outside the SVZ-RE area the radial glia was less regularly arranged, and a very faint GFAP immunoreactivity became detectable throughout the forebrain. Electron microscopy revealed the presence of isolated astrocytic-like processes randomly scattered in the mass of SVZ-RE neuroblasts, small aggregates of tightly apposed processes being rare (Fig. 4A,B). Cells different from the typical neuroblasts were also observed (Table 3), mostly at the periphery. Some of them had large cell bodies, with a lighter cytoplasm and more disperse nuclear chromatin than neuroblasts, thus likely corresponding to the transforming radial glia cells (Fig. 4C). In addition, some cells showing features similar to mature astrocytes (type-B cells of the adult) were also present, particularly in mice (Fig. 4D). The immature glial cell types represented 6.5% of the total cell population, whereas type-B cells only 0.8% (see Table 3).

Most of the radial glia fibers spanning the brain tissue had disappeared at P9, the immunoreactivity for vimentin now being mainly concentrated in the SVZ-RE area, with a distribution similar to that observed at P6, although better delineated: a dense meshwork of glial processes along the RE-OL, and a small-mesh net with numerous, thin glial processes in its inner part (not shown). At this stage, in rats, most of the vimentin-positive structures in the SVZ-RE were also immunoreactive for GFAP, although the former was primarily associated with large longitudinal processes, whereas the latter, similarly to nestin, revealed thinner glial ramifications.

At P13 the presence of astrocytes was clearly revealed by the GFAP staining in rats (Fig. 1, Table 1), whereas in mice the detection of the same antigen was delayed around P15 (Table 4). In both species the immunoreactivity for GFAP in the SVZ-RE was still associated with a fine meshwork of intermingled processes, in contrast with the typical stellate-shaped cells detectable in the mature forebrain tissue. This GFAP meshwork was particularly evident in the medial and ventral part, and delineated a high number of spaces which were not completely separated from each other (Figs. 1, 2). Although glial processes were frequently grouped to form short septa, no glial tubes were visible at this stage. The immunoreactivity for vimentin and nestin began to disappear from the surrounding forebrain tissue, although remnants of radial glia were visible in the tissue surrounding the SVZ-RE, at both the medial and lateral aspect. Starting from this stage the glial cell bodies revealed with BLBP and ALDC/ZII were more uniformly distributed through the whole SVZ-RE thickness, their accumulation at the RE-OL now being less evident.

TABLE 4. Single Important Events Detectable in the SVZ at Different Postnatal Stages and Their Correlation With Molecular Changes

		PSA-NCAM	Cx43	Ten-C
P0				+ (P)
P3	Radial glial arrangement replaced by homogeneous glial network (M&R) Closure of the olfactory ventricle (M)	+ (diffuse)	–	++ (P)
P6	Closure of the olfactory ventricle (R)			++ (P) (RE-OL)
P9	First GFAP$^+$ staining (R) Ten-C punctate staining disappears (M)			++ (D) (around cell masses)
P13				
P15	First GFAP+ staining (M) Inversion of PSA-NCAM staining (M&R) First appearance of chains (M)	++ (clustered)		
P17	Thick glial septa (R)		+	
P21	First appearance of chains (R) First appearance of glial tubes (R) Thick glial septa (M) Appearance of Cx43 in glial tubes (M&R)	+++ (chains)	++ (glial tubes)	+++ (D) (around chains)
P25	First appearance of glial tubes (M)		+++ (glial tubes)	+++ (D) (glial tubes)

(R) rat; (M) mouse; (P) punctate; (D) diffuse.

At P13, the ultrastructural analysis revealed a pattern similar to that observed at P6, with large masses of electron-dense neuroblasts, intermingled with immature glial elements (4.8%) and cells showing the ultrastructural aspect of mature astrocytes (2.4%) (Figs. 5B, 6A; Table 3). Nevertheless, unlike previous stages, the glial cells and processes were observed more frequently as aggregates (Fig. 5A) and to partially encircle groups of neuroblasts (Fig. 5B).

At P17 GFAP-positive stellate astrocytes were abundant throughout the brain, particularly in large bundles of white matter. The glial organization observed at P13 in the SVZ-RE was still present, but thicker septa corresponding to the close apposition of several processes emerged in the fine glial net and for the first time an organization reminiscent of glial tubes was visible in the medial part of the SVZ-RE (Fig. 1). This pattern coexisted with wide areas in which the neuronal precursors were not completely separated in clusters by the glial processes (Fig. 1), whereas some well-defined clusters were detectable in the SVZ-RE lateral part, close to the white matter. From P17 onward, the distribution of BLBP- and ALDC/ ZII-immunoreactive cells remained uniformly distributed in the SVZ-RE.

This organization strikingly changed at P21–25, when the fine glial net was completely replaced by thick, GFAP-positive septa delineating a series of rather homogeneous fields typical of adult glial tubes (Fig. 1). The immunoreactivity for vimentin at this stage was highly restricted to these glial structures in the SVZ-RE, having disappeared in the surrounding tissue. Electron microscopy confirmed the compartmentalization of the large masses of neuroblasts in chains made up of 5– 6 nucleated cells, now distinguishable from each other by the interposition of thick septa containing glial processes intermingled with the surrounding parenchyma (Figs. 5C,D, 6B). Some glial septa were formed by the close apposition of many astrocytic processes, but they were frequently associated with nerve fiber bundles (axons and dendrites), particularly in the lateral part (Fig. 5C,D). Thus, the chains appeared to be wrapped partially by glial processes and partially by parenchymal septa (Fig. 5C,D). The number of isolated glial processes appeared highly reduced in comparison with earlier stages. The ultrastructural semiquantitative analysis carried out at P21 indicated a further increase in the number of mature astrocytic cells (see Table 3).

At P30 the overall organization described at P21–25 was substantially unchanged in rats, whereas in mice a complete assembly of the glial tubes was slightly delayed. At subsequent stages no major differences were observed.

To confirm the identity of electron-lucent profiles as astrocytic processes, an ultrastructural immunogold staining for GFAP was carried out. Both in control specimens from adult brain tissue (Fig. 7C) and in the SVZ-RE of P21 animals (Fig. 7D) the immunostaining was specifically associated with typical “watery cytoplasm” glial cells and processes.

Species-specific antigenically different glial cell subpopulations

At early stages, BLBP and ALDC/ZII were observed in overlapping glial cell populations (Fig. 2F). At later stages, the BLBP+ cell population appeared reduced in mice, but not in rats (Fig. 2G,K). From P45 onward, only a few BLBP? cells were detectable in the mouse SVZ-RE, primarily localized at the RE-OL (Fig. 2G; Table 1). In GFAP/BLBP and BLBP/ZII double stainings only a partial colocalization of the two antigens was observed (Fig. 2G,I).

Remarkable differences between the two species studied were also observed by using the glial marker S100β. Most glial cells in the rat SVZ-RE were immunoreactive for S100β (and colocalized with BLBP and ALDC/ZII; Fig. 2K–M) throughout all the stages examined, whereas a few ramified glial cells were detected in mice (Fig. 2H; Table 1). In mice, these cells were primarily localized along the RE-OL and were mostly BLBP- and GFAP-negative. In adult animals, only some S100β+ elements were overlapping with the BLBP-immunoreactive small cell population (Fig. 2J). In BrdUrd-treated animals some BLBP+ and, to a lesser extent, S100β+ cells were shown to undergo DNA synthesis both in young (Fig. 8B,C) and adult (Fig. 8J,K) animals, thus suggesting that the small population of immature glial cells persisting in the SVZ-RE is dividing, at least partially.

Since qualitative and semiquantitative analyses indicated an overall increase of glial cells and their processes in the postnatal development of the SVZ-RE (see above), the occurrence of cell proliferation and gliogenesis across these stages was investigated.

Within the SVZ-RE a high rate of local cell proliferation, detected using Ki67 antigen and BrdUrd, revealed at 2 hours postinjection, was observed at all the stages examined, whereas it dramatically decreased in the surrounding forebrain tissue around the second/third postnatal week, then falling close to zero at P21.

The distribution of newly generated cells within the SVZ-RE was studied at different stages and at different postinjection survival times (see Fig. 8). Early postnatally, most of the cells divided along the RE-OL (Fig. 8A). In mice treated with BrdUrd at P3 and killed at P6, it appeared evident that most of these newly generated cells, identified by double labelings with β-tubulin in the SVZ- RE, moved centripetally and rostrally, to enter the RMS (Fig. 8D). On the other hand, in animals treated with BrdUrd at P3 and killed at P25, besides cells double-stained for BrdUrd/β-tubulin or/NeuN in the olfactory bulb (Fig. 8P) corresponding to rostralward migrating elements, some BrdUrd/S100β, /BLBP, and /GFAP double- stained cells were consistently detectable at all levels of the SVZ-RE (Fig. 8G–I), thus indicating the occurrence of newly generated, resident glial cells. Interestingly, most of these cells were still observed within the peripheral part of the SVZ-RE.

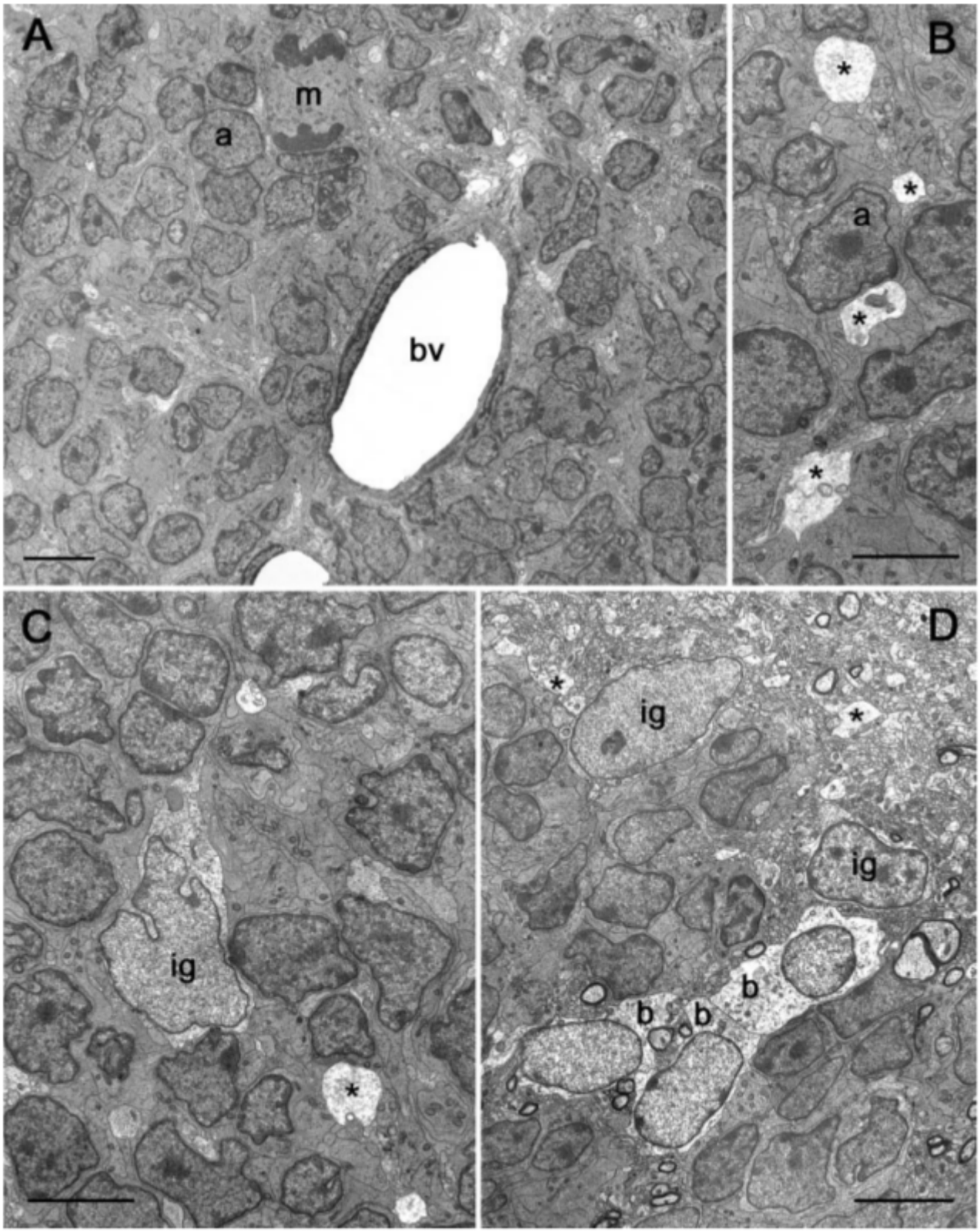

Fig. 4. Ultrastructural study of the early postnatal SVZ-RE (P6, coronal sections). A: Low magnification of the SVZ-RE showing the homogeneous mass of type A cells (a). These cells are in direct contact with blood vessels (bv), without the interposition of astrocytic processes; note the absence of intercellular clefts among the cells; m, mitosis. B: At this stage, only scattered astrocytic processes, recognizable for their clear cytoplasm (b, asterisks) are intermingled with the type A cells; note that most of them are single processes. C: Cells larger than type A cells and less electron-dense were interpreted as immature glia (ig). D: Cells with the morphology of mature astrocytes (b) were also observed (RE-OL; mouse). Scale bars =3 μm.

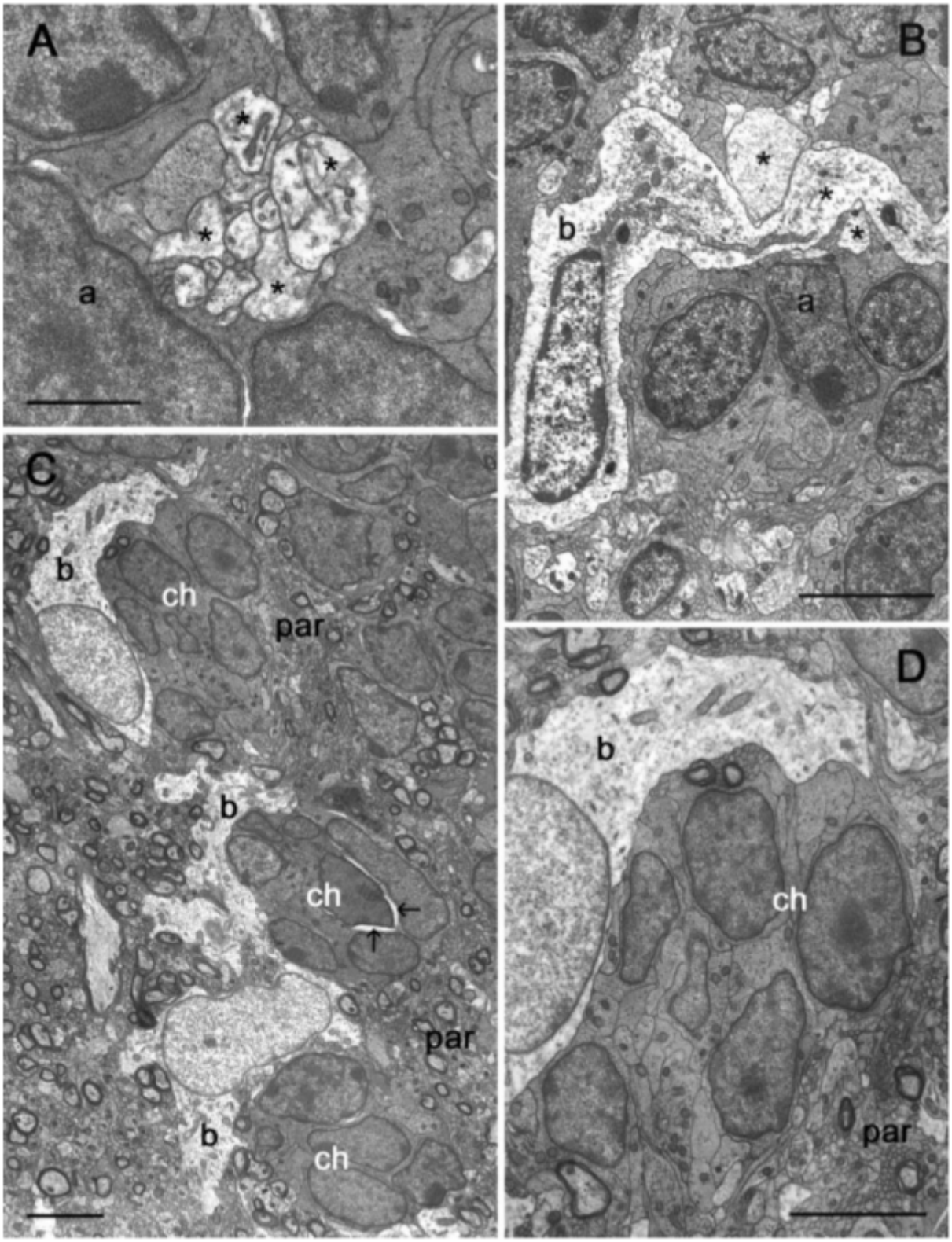

Fig. 5. Ultrastructural study of the postnatal SVZ-RE at P13 (A,B) and P21 (C,D); coronal sections. At P13, several astrocytic processes (b, only four larger processes are indicated) are frequently associated to form septa intermingled with the neuroblasts (type A cells, a) (A). Astrocytes and their processes start to encircle groups of neuroblasts (B). At P21 chains of neuroblasts (ch) are detectable, being en-sheathed by astrocytic processes (b) and parenchymal septa (par) (C, enlarged in D); note the appearance of intercellular clefts (arrows) among the neuroblasts. Scale bars = 1 μm in A; 3 μm in B–D.

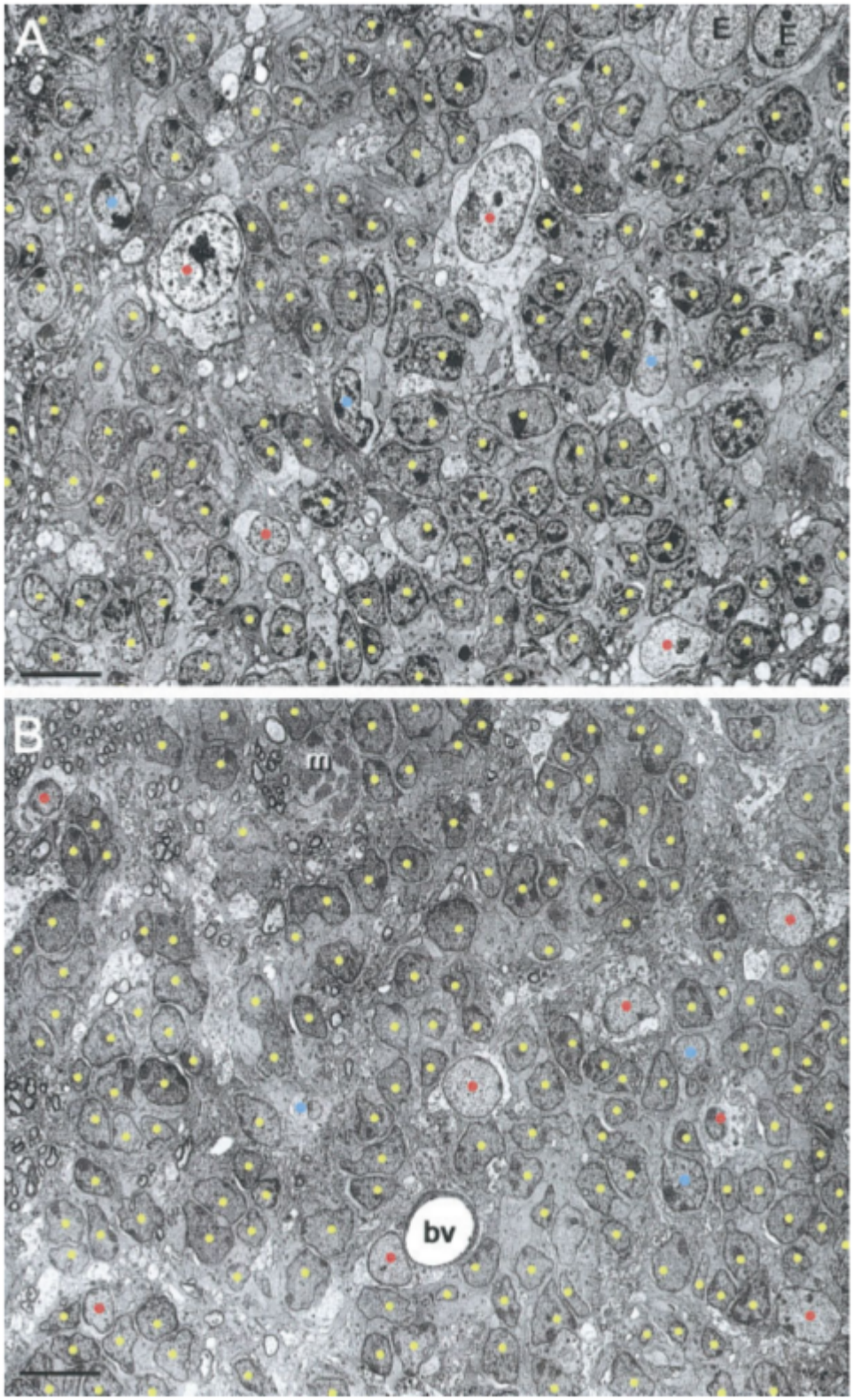

Fig. 6. Cell types of the postnatal SVZ-RE at the electron microscopic level (A: P13; B: P21). Low-magnification images of SVZ-RE coronal sections, containing type A cells (neuroblasts, yellow dots), type B cells (mature astrocytes, red dots), immature glial cells (blue dots), ependymal cells (E), and mitotic figures (m). bv, Blood vessel. Scale bars = 3 μm

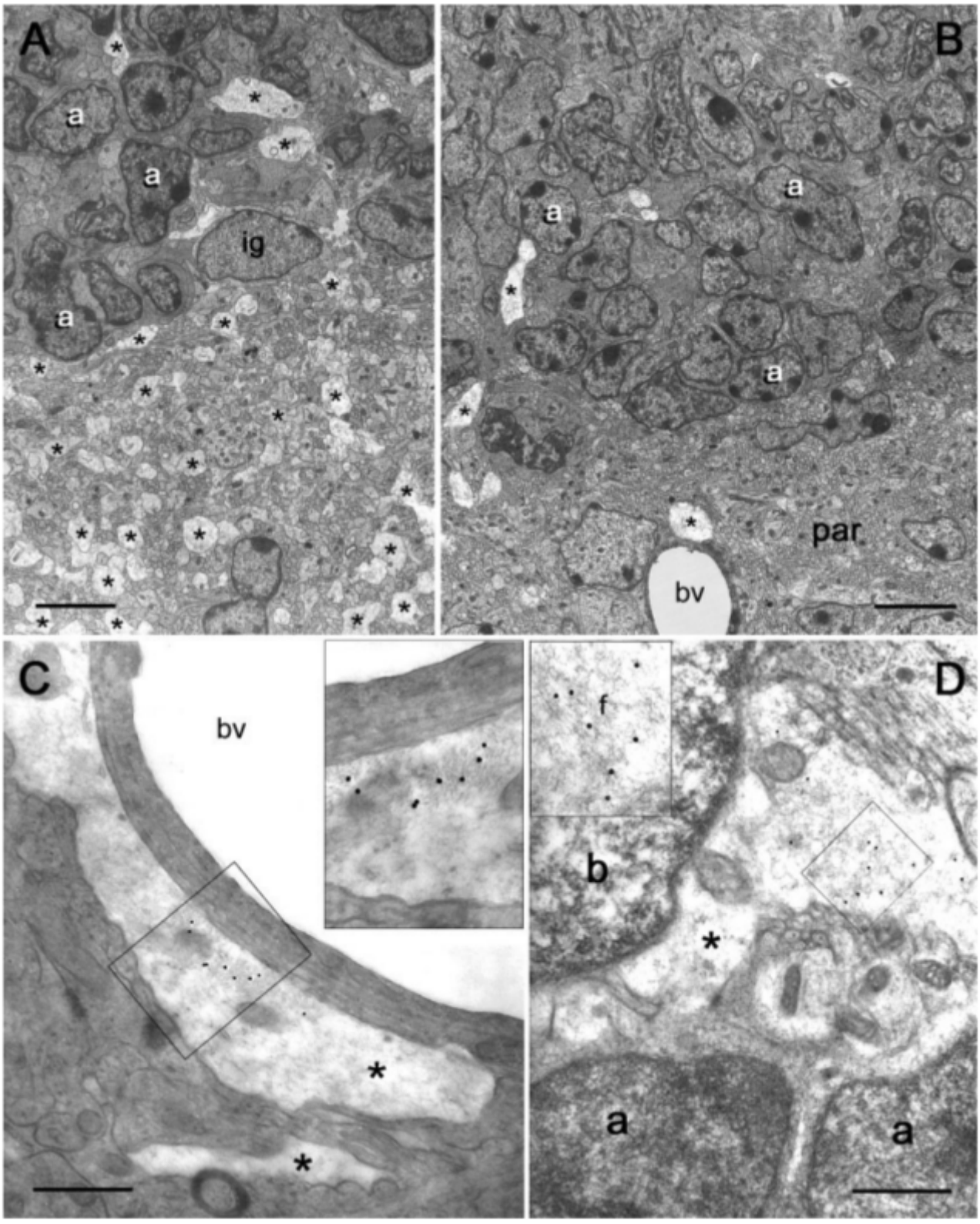

Fig. 7. A,B: Ultrastructure of the RE-OL (P6, coronal section). The homogeneous mass of neuroblasts (a, only some of them indicated) appears sharply delineated at the RE-OL, either in the presence (A, medial) or absence (B, lateral) of densely packed glial processes (some of them indicated by asterisks). The electron-lucent glial processes are easily recognizable from the parenchyma (par) of the surrounding tissue. bv, blood vessel. The areas shown correspond to the medial and lateral parts (here both at the bottom of the micrographs) of the RE-OL as shown in the schematic drawing of Figure 1. C,D: Postembedding immunogold staining for GFAP confirms the identity of electron-lucent ("watery cytoplasm") profiles as astrocytic processes. C: Astrocytic processes (asterisks) adjacent to a blood vessel (bv) in the adult rat. D: Astrocyte (type B cell, b) in the SVZ-RE of a P21 rat; note the immunostaining associated with glial filaments (f). a, type A cells. Scale bars = 3 m in A,B; 0.75 μm in C; 1 μm in D.

Neuroblast compartment

The migrating neuroblasts of the RMS (type-A cells in the adult) were easily identified throughout all the stages studied by using class III β-tubulin immunocytochemistry (Fig. 2D). On the other hand, the PSA-NCAM immuno-staining, although present during the whole postnatal life, displayed the typical features previously described in the adult (Bonfanti and Theodosis, 1994; Rousselot et al., 1995) only at later postnatal stages (see below). Electron microscopy confirmed that small/medium-sized neuroblast-like cells with a dark cytoplasm filled with free ribosomes form a homogeneous population maintaining its cytological features during the entire postnatal period (Figs. 4 –7). The ultrastructural analysis was used to study the relationships among these cells in order to reveal the occurrence of chains. At P6 a rather homogeneous cell mass virtually filled the SVZ-RE (Fig. 4). Consistent with light microscopic immunocytochemistry, only scattered astrocytic processes were intermingled among the neuroblasts. Apart from cells located at the RE-OL, which were in contact with either the surrounding parenchyma or the glial processes (Fig. 7; see below), most of the neuroblasts established direct mutual contact with one another. Their cell membranes were always in tight contact, not showing the typical intercellular clefts described in the adult RMS (Lois et al., 1996; Jankovski and Sotelo, 1996; Peretto et al., 1997). Moreover, they frequently appeared in direct contact with blood vessels, without the interposition of any astrocytic processes (Fig. 4). In mice, some masses and clusters reminiscent of future chains were already detectable at this stage, along the lateral part of the RE-OL, in the absence of any organized glial structure (Fig. 7B).

At P13, large masses of migrating neuroblasts were still present, only partially separated by the increasing astrocytic cells and processes (Fig. 5). These cell masses, particularly in the medial part of the SVZ-RE, appeared not as distinct chains, but rather largely intercommunicating. Some chains were already recognizable in the lateral part,ensheathed by scarce glial processes mixed with thick parenchymal septa.

Ultrastructural evidence for well-separated chains of neuroblasts characterized by wide intercellular clefts was observed in the P21 animals (Fig. 5C,D). At this stage, most of the neuroblasts adjacent to blood vessels were not in direct contact with endothelial cells, due to the presence of interposed glial processes (not shown).

Other cell types

In all three stages examined at the ultrastructural level, some intermediate forms with both type-A and type-B cell cytological features were intermingled among these two easily identifiable cell populations (Figs. 4C, 6). As described above, some of these cells have a cytoplasm darker than astrocytes and lighter than neuroblasts, and both cytoplasm and nuclear chromatin were more disperse. The intermediate forms were interpreted as immature glial cells gradually taking on the morphology of astrocytes (see Table 3). In addition, some larger cells were very similar to the so-called type-C cells described in the adult SVZ (Doetsch et al., 1997). In cell countings all these elements were considered as immature glial cells. Other cell types, quantitatively less important, were represented by micro- glial cells, ependymal cells, mitotic, and apoptotic figures (see Table 3). Ependymal cells were found at all three stages investigated (Fig. 6), but not taken into account, since their occurrence varied greatly due to the single tracts of the RE examined.

At P6, most of the elements with a medium degree of electron-density had large cell bodies (Fig. 4C). These types of cells were considered immature glial cells, probably corresponding to radial glia. At this stage a few cells (more frequently in mice) displayed features of mature astrocytes, with a “watery cytoplasm” (Fig. 4D). Starting from P13, the number of cells with intermediate features was lower, whereas that of astrocytic-like cells had increased (Table 3). The same trend was even more evident at P21, when the intermediate cells represented only 2.4%.

SVZ-RE outer limit (RE-OL)

Since many changes described in this study occurred at the interface between the SVZ-RE and the surrounding parenchyma, they are worth a separate description. The RE-OL was clearly recognizable at all the postnatal stages investigated, although for very different aspects. As also described by Alves et al. (2002), starting from P3– 6 radial glial processes were observed to change their radial orien- tation in correspondence of the RE-OL (see Figs. 1, 3). At this level they were frequently grouped in thick fascicles which assumed a tangential orientation in contrast with the random distribution of the thin mesh net detectable in most of the SVZ-RE between P6 and P13 (Fig. 3). The accumulation of glial processes at the RE-OL was accompanied by a higher density of cell bodies, as revealed by BLBP and ALDC/ZII immunocytochemistry (Fig. 2). All these events were particularly evident on the medial side, and were observed on short tracts of the RE-OL early postnatally, then becoming progressively more extended at later stages. During the second postnatal week, the tangentially oriented fascicles of radial glia apparently delineated the external perimeter of the SVZ-RE, thus starting to separate the mass of migrating cells from the surrounding forebrain tissue.

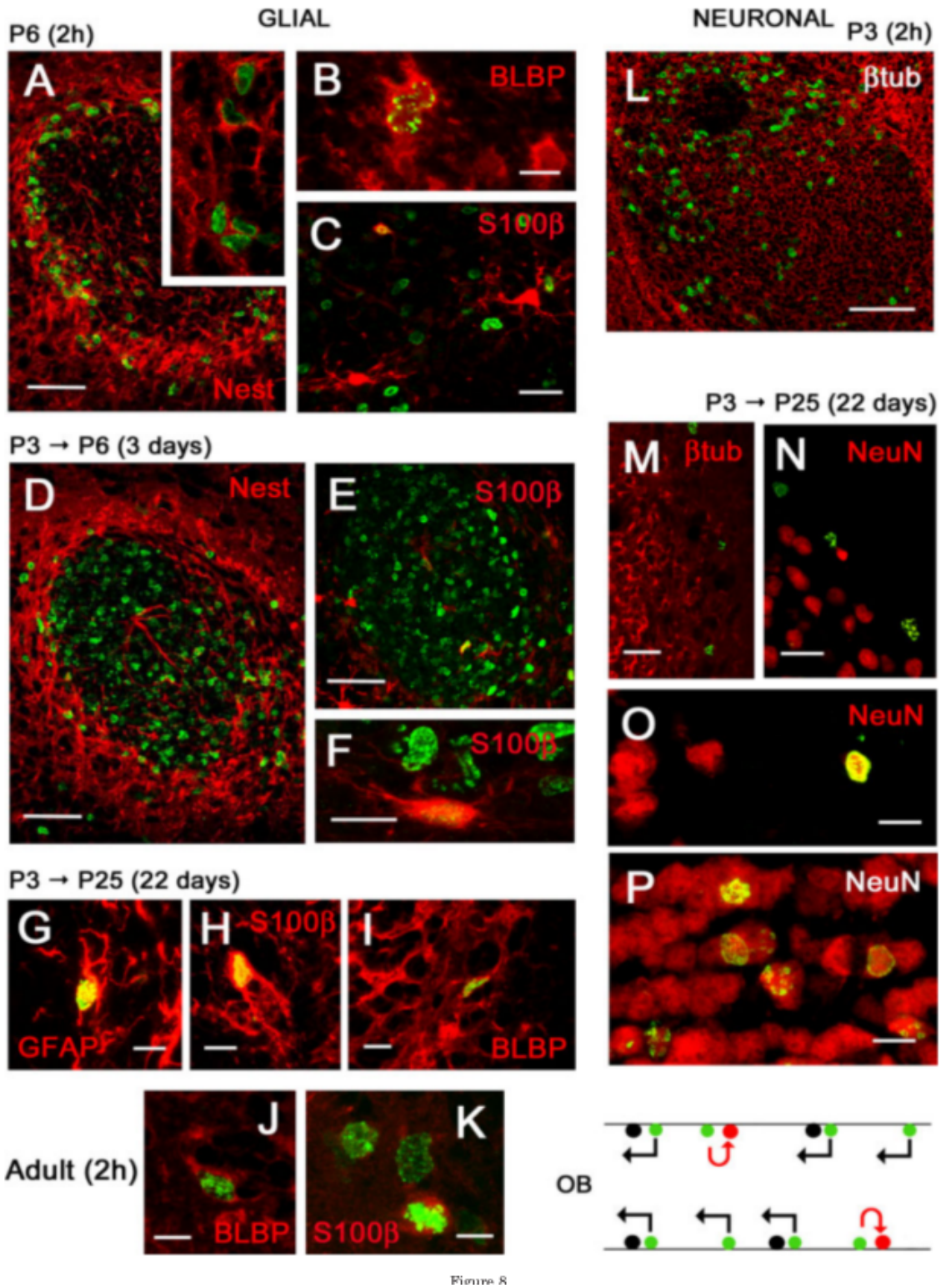

Fig. 8. Cell proliferation, gliogenesis, and neurogenesis in the postnatal SVZ-RE, revealed with BrdU staining (green) in association with glial (left) and neuronal (right) markers, at different postinjection survival times. Early postnatal cell proliferation is concentrated at the periphery of the SVZ-RE (A,L). Within a short period (from P3 to P6), most of the cells migrate as neuroblasts towards the SVZ core (D) and, in a longer period of time (from P3 to P25) to the olfactory bulb (M,P). A population of nonneuronal cells also is generated (M,N), partially involving the S100β+ and BLBP2 cells (B,C,E,F). Some newly generated glial cells remain resident in the SVZ-RE after 22 days (G–I; micrographs obtained from the RE-OL) and some are still dividing in the adult (J,K). The fate of the newly generated cells in the postnatal SVZ-RE is summarized in the drawing (bottom right): black dots, preexisting glial cells; green dots, cell proliferation; black arrows, newly generated neuroblasts directed to the olfactory bulb (OB); red dots, newly generated, resident glial cells. Scale bars = 50 μm in A,D,E,L; 10 μm in B,F–K,M; 20 μm in C,N–P.

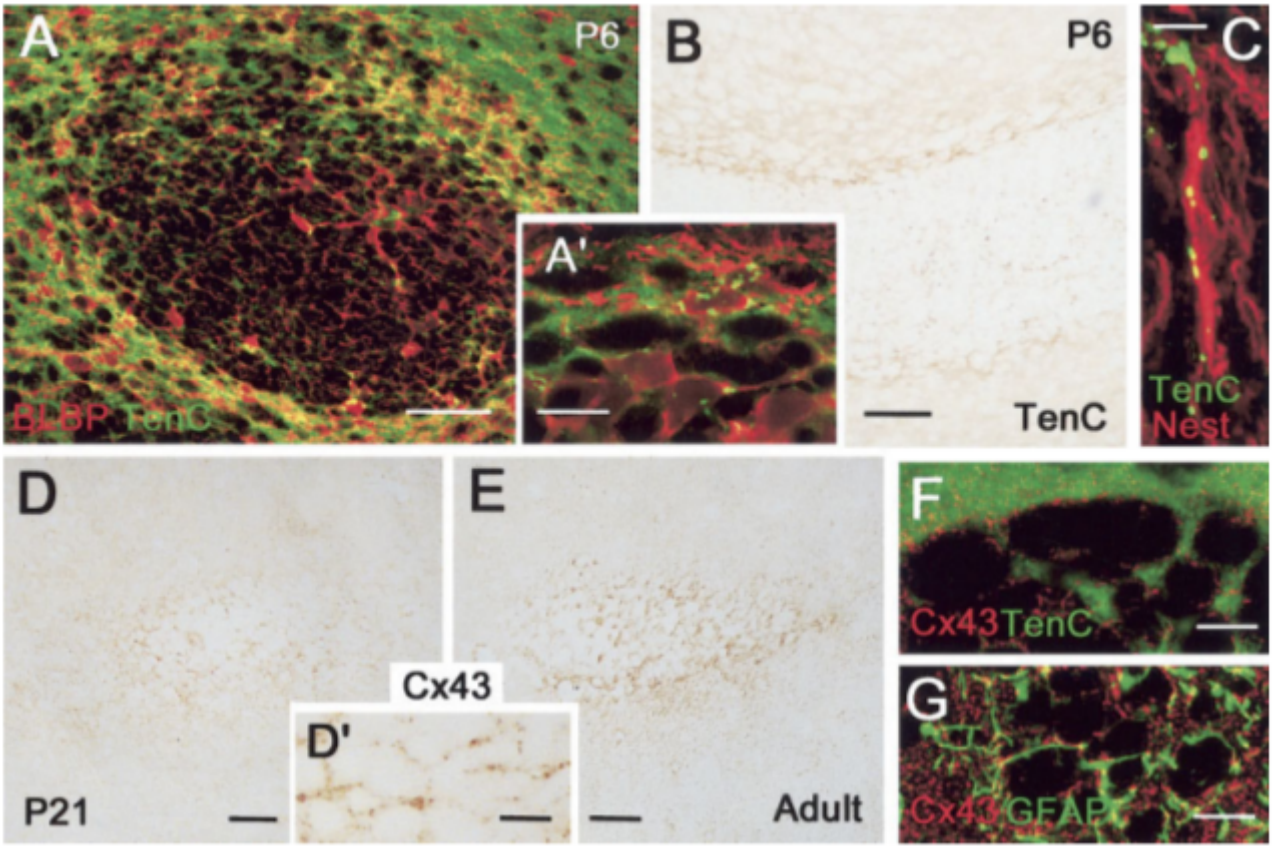

Fig. 9. Detail and double stainings for tenascin-C, Cx43, and other antigens. At P6, tenascin-C is present as a punctate reaction in the radial glia cells on the RE-OL (A,A',C, yellow dots in confocal images from double stainings), whereas it is diffuse in the extracellular matrix of the surrounding tissue (A: green; B: brown, sagittal section). Astrocytic gap junctions are detectable in the SVZ-RE starting from the third postnatal week (D) and are abundant in the adult SVZ (E), associated with the glial tube outline (D') as confirmed by double stainings with tenascin-C (F) and GFAP (G). Scale bars =50 μm in A,B,D,E; 10 μm in AJ,F,DJ,G; 5 μm in C.

The details concerning the interface between migrating neuroblasts and surrounding tissue in the absence of glial tubes were investigated by electron microscopy. At P6, and to a lesser extent at P13, a direct contact between the
mass of neuroblasts and the surrounding parenchyma was observed to occur (Fig. 7B). This was observed particularly on the lateral part of the SVZ-RE, in contact with the
white matter. On the other hand, in the medial part of the perimeter a high density of astrocytic cells and processes was interposed between the neuroblasts and the parenchyma (Fig. 7A). Some clusters of neuroblasts, as well as isolated cells, were occasionally observed beyond the RE-OL, completely immersed in the surrounding parenchyma (not shown). During these early stages the RE-OL also represented a border line for the proliferative activity detected at different postnatal stages (see below). Starting from P21, astrocytic cells and processes were observed to form a relatively continuous barrier between the neuroblasts and the surrounding parenchyma.

PSA-NCAM, tenascin-C, and Cx43 immunostainings

In the stages between P0 and P13, a widespread and diffuse immunostaining for PSA-NCAM was detectable both in the SVZ-RE and in the forebrain parenchyma, appearing even more intense in the latter (Table 4; Figs. 1, 10). In the rat, starting from P17, and more evident at P21, a dramatic decrease in polysialic acid content was observed in regions located outside the SVZ-RE, whereas

the staining was now very intense within the SVZ-RE area (Fig. 1I,L). In the mouse, the same shift was observed starting from P15 (Table 4). Across these stages, the distribution of PSA-NCAM within the SVZ-RE gradually changed from a diffuse staining associated with the mass of uniformly arranged cells (up to P13), to a more specific expression on some cell aggregates (at P15 in mice and P17 in rats) and to the chains of cells (starting from P21; Figs. 1L,O, 10). At the level of the RE-OL, some PSA- NCAM-positive cells arranged in clusters were already detectable at P6 –9.
The immunocytochemical labeling for tenascin-C was detectable at all the stages investigated, but with a strikingly different distribution (summarized in Table 4 and Fig. 10). As previously shown (Gates et al., 1996), during the early postnatal period (P0 – 6) tenascin-C was detectable both inside and outside the SVZ-RE (Fig. 1). A strong punctate reaction was present within the SVZ-RE, in sharp contrast with the diffuse immunostaining of the surrounding brain parenchyma (Figs. 1, 9). This latter was a typical intercellular staining, the large neuronal cell bodies remaining completely unstained. By contrast, the punctate reaction for tenascin-C was contained into radial glia cell bodies and processes, in the form of large vesicles, as visible in nestin/tenascin-C or BLBP/tenascin-C double stainings (Fig. 9). This punctate reaction did not correspond to transversely sectioned cell processes, since it appeared similar also in longitudinal views and thick vibratome sections. Across the second postnatal weeks most of the punctate and diffuse immunoreactivity for tenascin-C progressively concentrated at the RE-OL (Figs. 1, 9, 10). Starting from the third postnatal week, no more punctate reaction was detectable, whereas the diffuse staining was associated with the outline of the assembling chains of neuroblasts in the lateral part of the SVZ-RE, wherein glial septa were not yet assembled (Figs. 1, 10). At P25–30 a halo of tenascin-C diffuse staining was still present on the RE-OL, overlapping with the glial tube perimeter (Fig. 9F). As previously described (Jankovski and Sotelo, 1996), after the end of the first month tenascin-C was not detectable outside the SVZ-RE area, nor in association with the chains of cells, a diffuse intercellular staining being highly restricted to the contour of the glial tubes.
The distribution of the astrocyte-specific gap-junctions connexin (Cx-43) was analyzed both in the adult and post- natal rat and mouse forebrain. In the adult, as previously described (Yamamoto et al., 1990), a widespread immunoreactivity for Cx-43 was consistently detected both in gray and white matter in the form of a punctate reaction (not shown). A higher density of immunoreactivity was observed in the SVZ-RE area, specifically concentrated in correspondence with the glial tubes wall (Fig. 9E). Double labeling for Cx-43 and GFAP confirmed the coexistence of the two antigens in the astrocytic meshwork forming the tubes (Fig. 9G), taking into account the membrane-bound localization of the former and the cytoskeletal one of the latter. In postnatal animals no Cx-43 immunoreactivity could be detected up to P17, when it appeared as very faint punctate reaction in the SVZ-RE, in correspondence with the assembling glial septa (Table 4). A consistent immunoreactivity, similar to that described in the adult, was first detected in the SVZ-RE at P21 (Fig. 9D), although at this stage only scarce punctae were detected in the surrounding forebrain tissue.
These results show that the distribution of adhesion and boundary-linked molecules appear to be somehow inverted in the shift from postnatal and adult SVZ, whereas Cx-43 is highly detectable within the SVZ-RE in sharp coincidence with the glial tube assembly.

DISCUSSION

In the present study, a detailed analysis of cell composition, overall organization, and molecular characterization of postnatal rodent SVZ-RE has confirmed that striking differences do exist on comparing early postnatal and adult animals. Most changes involved in this transformation are temporally restricted to the first three postnatal weeks (summarized in Table 4), leading to the assumption that after this period the SVZ of “young” animals is qualitatively comparable with that of adults. From the anatomical point of view, no substantial differences were observed comparing mice and rats, although a slight temporal delay was observed in the former as regards glial structure

assembly, in spite of its earlier and faster perinatal development. On the other hand, interspecific differences have been found in the molecular profile of certain glial cell populations.
As considered in previous studies (Kishi, 1990; Luskin, 1993; Alves et al., 2002; Tramontin et al., 2003), the most striking differences between postnatal and adult SVZ concern cell migration and glial organization. Thus, we examined the replacement of a massive tangential migration, orthogonal to radial glia processes, with a tangential "chain" migration through longitudinally oriented glial tubes. Our results will be discussed by splitting this period into two parts: 1) early postnatal period (first 10 days), in which glial cells are not organized; and 2) subsequent postnatal events (from P11–21), corresponding to the assembly of glial tubes and chain formation.

Early postnatal period: tangential cell migration in the absence of glial tubes

During the first week after birth, although a great number of small glial processes were detectable in the SVZ-RE, the migrating neuroblasts formed large, rather uniform or widely intercommunicating masses. Electron microscopy confirmed that most of these cells are in contact with one another, with the occasional interposition of glial processes. This arrangement is very different from the typical chain organization of adult SVZ, in which large portions of neuroblast cell surface come into contact with astrocytes (Lois et al., 1996; Jankovski and Sotelo, 1996; Doetsch et al., 1997; Peretto et al., 1997). Besides previous light microscopic observations in vivo (Alves et al., 2000; Pencea and Luskin, 2003) and in vitro studies (Mason et al., 2001; Murase and Horwitz, 2002) which proposed that tangential chains can occur very early in RMS, even during embryogenesis, our ultrastructural analysis, allowing the visualization of all cell types, indicate that no chains are present in SVZ-RE until later stages. Although a higher density of glial cells and processes can be observed along certain tracts of the RE-OL, they do not provide a continuous coverage, as migrating neuroblasts are allowed to be at times in direct contact with surrounding parenchyma. Moreover, at the external limit of the uniform cell mass, single and aggregated elements immersed in the adjacent tissue beyond the RE-OL can also be observed. This "leaky scaffold" occurs particularly in the lateral part of the SVZ- RE, at the interface with the white matter, where some glial cell precursors are known to leave the stream in the early postnatal period (Marshall et al., 2003). Interestingly, in the SVZ-RE most of neuroblasts adjacent to blood vessels were in direct contact with the endothelial wall, whereas in the adult the chains are known to be separated from blood vessels by the interposition of astrocytic processes, a direct contact with endothelial cells being occasional (Peretto et al., 1999). Taken together, these observations suggest that cell migration at this stage occurs somehow independently from the presence of glial structures, both within the SVZ-RE and at its outer limit. For these reasons, the conclusion of Alves et al. (2002) that "transforming radial glia provide a glial ensheathment of the SVZ/RMS in the early postnatal animal, similar to the adult astrocytic sheath," should be considered true only for the medial part of the RE-OL. This does not mean that glial cells could not play an indirect role in such a process, since their involvement in "glial related activities" as a source of extracellular matrix molecules, trophic factors, and other alternative signaling functions is well known (Gates et al., 1995; Brannon Thomas et al., 1996; Jankovski and Sotelo, 1996; Goldman and Luskin, 1998; Peretto et al., 1999; Mason et al., 2001; Pencea and Luskin, 2003; Bolteus and Bordey, 2004; Peretto et al., 2004).

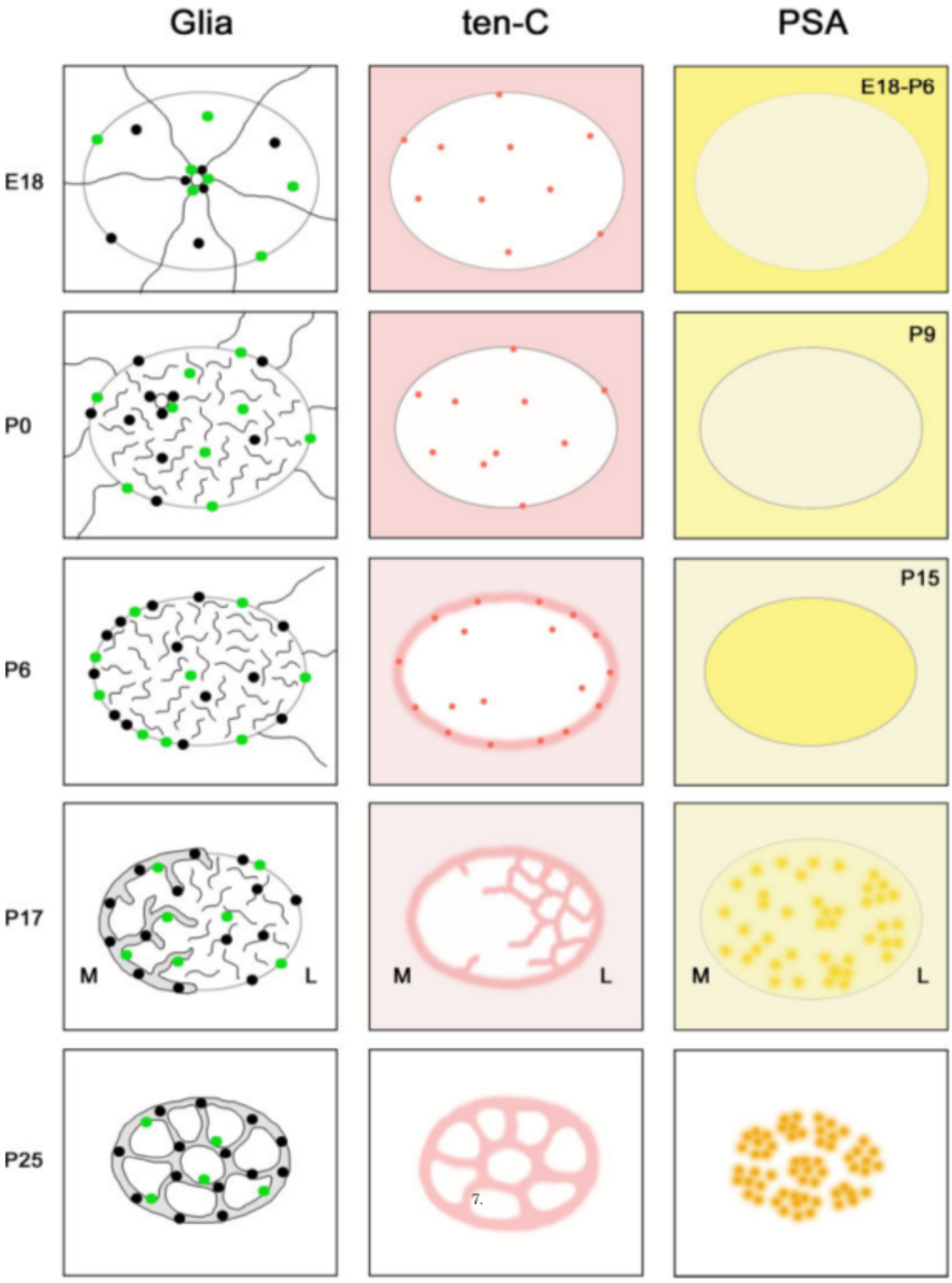

Fig. 10. Schematic representation of morphological and molecular changes occurring in the shift from postnatal to adult SVZ-RE (coronal views). Note the changes in the relative amount and spatial distribution of cell proliferation (green dots) and glial cell bodies (black dots) at the periphery or in the core of the SVZ-RE (left column). Glial cell processes (black lines) change from radial glial fibers (long lines), to a dense mesh net (short lines) and glial tubes (double lines with gray). The progressive organization of the glial processes seems to be associated with the compartmentalization of the mass of migrating neuroblasts (white) into chains (see text). These changes occur in parallel with an inversion of the distribution of PSA-NCAM (yellow, right column) and with the progressive concentration of tenascin-C (pink) on the glial tube/chains interface (middle column). Note also the progressive disappearance of the diffuse tenascin-C and PSA-NCAM immunoreactivities from the surrounding brain parenchyma. An asymmetry between the glial assembly (earlier in the medial part, M) and the chain formation (earlier in the lateral part, L) is visible around P17.

Early postnatal, primarily glial-independent cell displacement is likely to involve different cell-to-cell contacts and affinity compared with the adult, as also suggested by the distribution of PSA-NCAM at these postnatal stages. In the past, this adhesion molecule enriched in polysialic acid was referred to as an “embryonic” form of N-CAM (Rougon et al., 1986) due to its abundance in developing CNS and to its spatially restricted distribution in adult brain structurally plastic/neurogenetic sites (Bonfanti et al., 1992; Bonfanti and Theodosis, 1994). The distribution of PSA-NCAM in the SVZ-RE during the first two postnatal weeks, even less abundant than in surrounding forebrain tissue, could suggest that this molecule is less important for early occurring, massive cell migration, than for adult chain migration. Nevertheless it must also have a role in the postnatal SVZ cell displacement, since previous studies showed that its removal does actually inhibit migration at this stage (Ono et al., 1994; Hu et al., 1996). Even the absence of intercellular clefts typically described in the adult at the interface of SVZ neuroblasts (Lois et al., 1996; Jankovski and Sotelo, 1996; Doetsch et al., 1997; Peretto et al., 1997) supports the idea of different dynamics for early postnatal cell migration. Accordingly, the extracellular matrix molecule tenascin-C showed a sharply different distribution inside and outside the early postnatal SVZ. Tenascin-C is highly expressed during CNS development, primarily concentrated in transient boundaries around emerging functional units (Steindler et al., 1998; Garwood et al., 2001). In the postnatal SVZ-RE, it was restricted to radial glia cell bodies and processes, being absent in those parts of the same cells located beyond the SVZ-RE area. Since it is known that this glyco-protein is synthesized and released by young astrocytes, this pattern strongly suggests that tenascin-C is produced by SVZ-RE radial glia but not released into the RMS at these stages. Thus, tenascin-C does not appear to be involved in RMS early cell migration, but rather it might establish a molecular interface with the surrounding brain tissue at the RE-OL level, during those stages when a complete glial sheath is not yet present.

Subsequent postnatal period: assembly of glial tubes and chain formation

Previous studies carried out on postnatal mice (Alves et al., 2002) showed that radial glia undergoes changes as to shape and orientation, to eventually transform into adult SVZ astrocytes. Our results confirm that radial glial cells had already started to transform into astrocytes during the first 10 days of life, by increasing their ramifications in the SVZ-RE and by changing the orientation of their processes from radial to tangential along the RE-OL. Nevertheless, SVZ compartmentalization in glial tubes and chains of neuroblasts occurs later. Electron microscopy clearly showed that glial processes progressively assemble to form thicker septa, which eventually join septa of mature parenchyma (mainly axons) to ensheath chains during the third to fourth postnatal week. Immunoreactivity for Cx43, a protein heavily expressed in astrocytic gap junctions (Yamamoto et al., 1990; Theis et al., 2003), although present in the CNS since early stages (see also Nadarajah et al., 1997; Menezes et al., 2000), was extensively detected in sharp coincidence with astrocytic tube assembly. The massive appearance of Cx-43 astrocytic gap junctions in the SVZ around P21 supports the idea of a further stabilization of the glial compartment in the perspective of isolating the neurogenetic area from mature parenchyma. Nevertheless, it is important to stress that the age-related progressive increase in the relative amount of glial processes and in their degree of aggregation does not lead to complete wrapping of the first chains, which at P21 is still largely obtained by parenchymal septa. Moreover, by comparing SVZ-RE medial and lateral aspects, between stages P6 and P17, it appears evident that glial cells and processes were most abundant and tightly packed along the medial part. On the lateral side, in contact with the white matter, they consistently aggregated starting from P21–25, so as to form a glial mesh- work homogeneously distributed in the whole SVZ area. Starting from P13, electron microscopy allowed the first detection of chains on the lateral part of the SVZ-RE, namely, in the area where astrocytic processes are less aggregated, and where these first chains were also largely wrapped by parenchymal septa. Interestingly, a similar medial/lateral asymmetric distribution was observed by following the

temporal pattern of molecular expression, which also remarkably changed during the same period. An intercellular diffuse pattern of tenascin-C delineating the contours of cell masses replaced the vesicle-restricted reaction typical of early postnatal SVZ. In spite of its glia-related nature, the occurrence of tenascin-C was not strictly associated with an earlier assembly of glial septa in the medial part of the SVZ; rather, it was more evident in its lateral part, marking the perimeter of the first chains of neuroblasts. Indeed, the events described above occur slightly after a striking inversion of the pattern of PSA-NCAM immunoreactivity, which disappears from mature forebrain but is detectable in close association with assembling chains of neuroblasts around the third postnatal week. This observation is in accord with the fact that a high expression of PSA-NCAM would be essential for establishing and maintaining chain migration in the adult (Hu, 2000).
Thus, both morphological and molecular analyses strongly indicate that formation of chains is not directly linked to the glial organization process, but seemingly to molecular events, such as expression on the cell surface and in extracellular matrix.

Cell types, cell proliferation, and antigenically different cell populations during the postnatal period

Parallel to the assembly of glial tubes and chains, changes in the identity of different SVZ cell populations and subpopulations were also observed. Besides a remarkable homogeneity of neuronal precursors, whose changes were restricted to their mutual relationships, substantial differences were detectable as regards glial cell populations. During the progressive transformation of radial glia cells in more mature glial forms, a change was observed in the distribution of glial cell bodies: from ventricular position in embryogenesis to an accumulation along the RE-OL early postnatally, then to a more uniform distribution in the adult (summarized in Fig. 10). Both electron microscopy and immunocytochemistry showed that mature and immature glial cells coexist at different stages, with a progressive increase of mature astrocytic-like cells during postnatal development. Our results confirmed the prevalent segregation of S-phase cells on the external border of the SVZ (RE-OL) between the first and second postnatal weeks, as previously described by Menezes et al. (1998). In addition, it appeared clear that some glial cell precursors are generated in the postnatal SVZ, and that they remain resident inside the SVZ itself, in accord with qualitative and quantitative analyses. Thus, postnatal gliogenesis in the SVZ does contribute to the formation of glial tubes and (indirectly) to the compartmentalization of the migrating chain system. Most glial cells which are generated on the SVZ peripheral border maintain this position. Considering that from P13 onward astrocytes are distributed more homogeneously through the SVZ-RE, it might be hypothesized that glial cells directly deriving from radial glia transformation are primarily located in the central part of the SVZ-RE.
The occurrence of a slow gliogenesis in the postnatal SVZ could be important in establishing heterogeneous glial cell populations in this neurogenetic area. In mice, as demonstrated in this study, the RE-OL is characterized by the persistence of BLBP+ and S100β+ cell subpopulations, which are still detectable and proliferate during adulthood. In the hippocampus of adult mice the putative astrocyte-like progenitors are consistently S100β- negative, and no S100β+ cells can be found in S-phase (Steiner et al., 2004). Indeed, the proliferating S100β+ cells in the adult SVZ were rare.
These results, although leaving open the issue of which glial cells actually correspond to the adult SVZ neural stem cells, clearly show that specific subpopulations can exist in this adult germinative area and that postnatal gliogenesis in the SVZ might be involved in delineating glial cell subpopulations displaying different molecular profiles and a different degree of immaturity.

CONCLUDING REMARKS

Our observations lead to the conclusion that glial tube assembly and chain formation are the result of complex modifications occurring in the SVZ-RE during the first three postnatal weeks and characterize the shift from an embryonic- to an adult-like appearance of the SVZ. This temporal pattern coincides with full maturation of brain tissue at the end of neurogenesis, thus suggesting that the characteristic arrangement of adult SVZ (and in particular of its glial compartment) might mainly have a role in isolating the immature environment/stem cell niche of the SVZ from surrounding mature tissue. As to this interpretation, glial cells would not exert a direct role in cell migration, although one cannot exclude an indirect influence on cell displacement as a result of "glial-related activities." Although modifications in cellular composition and arrangement coincide with a different type of migration (chain migration), by following the above-discussed concept we do not consider the new arrangement essential for cell migration itself, but rather a means to allow an adaptation of embryonic/postnatal modes of cell migration to the mature nervous tissue substrate replacing the immature, more permissive environment. The typical clefts among neuroblasts of the adult SVZ previously described in ultrastructure (Lois et al., 1996; Jankovski and Sotelo, 1996; Peretto et al., 1997) also appear around P21. These clefts, which were interpreted as a technical artifact linked to the existence of wider intercellular spaces among migrating neuroblasts (Peretto et al., 1999) have not yet found a functional explanation. The present study shows that their appearance is temporally linked to SVZ compartmentalization in chains and glial tubes, supporting the hypothesis of a striking change in the dynamics of cell migration at this very stage. Indeed, the high expression of low-adhesive polysialic acid on fast-migrating cells contained within a semi-rigid system of astrocytes might explain the occurrence of enlarged intercellular spaces (see also Yang et al., 1992).

We show that in the early postnatal period radial glial cells and their processes do not provide a complete glial ensheathment to the young SVZ/RMS and no evident chains can be detected up to the third postnatal week. On the other hand, we do agree with previous studies (Alves et al., 2002; Pencea and Luskin, 2003) about the role played by tangentially oriented fascicles of radial glia fibers along the RE-OL in starting the process of glial tube formation, which eventually leads to SVZ/mature tissue separation. In this context, the assembly of glial tubes, although apparently linked to the compartmentalization of the migrating mass into chains, could be a subsequent event, as it is more evident in mice. The evident asymmetry between the medial and lateral parts of the SVZ-RE (summarized in Fig. 10) regarding different temporal patterns in the assembly of glial tubes (earlier in the medial part) and chains (earlier in the lateral part) supports this view. Our results suggest that changes in molecular expression of SVZ cells and extracellular matrix could be more likely involved in the regulation of cell migration rather than glial cells themselves. Indeed, several lines of evidence from in vivo (this study) and in vitro (Wichterle et al., 1997) studies indicate that chain migration is not necessarily linked to the presence of glial elements, an assumption confirmed by our recent in vivo demonstration that glia-independent chains of neuroblasts can be found outside the SVZ of mammalian species, even in the adult (Luzzati et al., 2003).

In conclusion, cell migration and glial cell types, two aspects mostly involved in the time-related changes of the SVZ, appear to be deeply intermingled but not directly related in a cause/effect way. A tentative explanation could be that they reflect in a different manner their adaptation to the maturing nervous tissue, both changing their pattern during a very narrow, but not completely overlapping, temporal window.

On these bases, we suggest that the adult SVZ should not be considered as a remnant of primitive periventricular germinal layers persisting into adulthood, but rather as a complex modification of a germinal layer which has progressively adapted to the mature brain environment.

ACKNOWLEDGMENTS

We thank T. Anthony for anti-BLBP, R. Bruzzone for anti-Cx43, G. Rougon for anti-PSA-NCAM, and R. Hawkes for anti-ALDC/ZII antibodies. We thank R. Bruzzone for stimulating discussion on connexins and G. Zanutto for expertise in graphics.

LITERATURE CITED

Altman J. 1969. Autoradiographic and histological studies of postnatal neurogenesis. IV. Cell proliferation and migration in the anterior forebrain, with special reference to persisting neurogenesis in the olfactory bulb. J Comp Neurol 137:433– 457.

Alves JAJ, Barone P, Engelender S, Froes MM, Menezes JRL. 2002. Initial stages of radial glia astrocytic transformation in the early postnatal anterior subventricular zone. J Neurobiol 52:251–265.

Bolteus AJ, Bordey A. 2004. GABA release and uptake regulate neuronal precursor migration in the postnatal subventricular zone. J Neurosci 24:7623–7631.

Bonfanti L, Theodosis DT. 1994. Expression of polysialylated neural cell adhesion molecule by proliferating cells in the subependymal layer of the adult rat, in its rostral extension and in the olfactory bulb. Neuroscience 62:291–305.

Bonfanti L, Olive S, Poulain DA, Theodosis DT. 1992. Mapping of the distribution of polysialylated neural cell adhesion molecule throughout the central nervous system of the adult rat: an immunohistochemical study. Neuroscience 49:419 – 436.

Boulder Committee. 1969. Embryonic vertebrate central nervous system: revised terminology. Anat Rec 166:257–261.

Brannon Thomas L, Gates MA, Steindler DA. 1996. Young neurons from the adult subependymal zone proliferate and migrate along an astrocyte, extracellular matrix-rich pathway. Glia 17:1–14.

Doetsch F, Garcia-Verdugo JM, Alvarez-Buylla A. 1997. Cellular composition and three-dimensional organization of the subventricular germinal zone in the adult mammalian brain. J Neurosci 17:5046 –5041.

Doetsch F, Caille I, Lim DA, Garcia-Verdugo JM, Alvarez-Buylla A. 1999. Subventricular zone astrocytes are neural stem cells in the adult mammalian brain. Cell 97:703–716.

Feng L, Heintz N. 1995. Differentiating neurons activate transcription of the brain lipid-binding protein gene in radial glia through a novel regulatory element. Development 121:1719 –1730.

Gaiano N, Nye JS, Fishell G. 2000. Radial glia identity is promoted by Notch1 signaling in the murine forebrain. Neuron 26:395– 404.

Garwood J, Rigato F, Heck N, Faissner A. 2001. Tenascin glycoproteins and the complementary ligand DSD-1-PG/phosphacan structuring the neural extracellular matrix during development and repair. Restor Neurol Neurosci 19:51– 64.

Gates MA, Brannon Thomas L, Howard EM, Laywell ED, Sajin D, Faissner A, Gotz B, Silver J, Steindler DA. 1995. Cell and molecular analysis of the developing and adult mouse subventricular zone of the cerebral hemispheres. J Comp Neurol 361:249 –266.

Giacobini P, Kopin AS, Beart PM, Mercer LD, Fasolo A, Wray S. 2004. Cholecystokinin modulates migration of gonadotropin-releasing hormone-1 neurons. J Neurosci 24:4737– 4748.

Goldman SA, Luskin MB. 1998. Strategies utilized by migrating neurons of the postnatal vertebrate forebrain. Trends Neurosci 21:107–114.

Gritti A, Bonfanti L, Doetsch F, Caille I, Alvarez-Buylla A, Lim DA, Galli R, Verdugo JM, Herrera DG, Vescovi AL. 2002. Multipotent neural stem cells reside into the rostral extension and olfactory bulb of adult rodents. J Neurosci 22:437– 445.

Hartfuss E, Galli R, Heins N, Gotz M. 2001. Characterization of CNS precursor subtypes and radial glia. Dev Biol 229:15–30.

Hu H. 2000. Polysialic acid regulates chain formation by migrating olfactory interneuron precursors. J Neurosci Res 61:480 – 492.
Hu H, Rutishauser U. 1996. A septum-derived chemorepulsive factor for migrating olfactory interneuron precursors. Neuron 16:933–940.
Jankovski A, Sotelo C. 1996. Subventricular zone-olfactory bulb migratory pathway in the adult mouse: cellular composition and specificity as determined by heterochronic and heterotopic transplantation. J Comp Neurol 371:376 –396.
Kishi K, Peng JY, Kakuta S, Murakami K, Kuroda M, Yokota S, Hayakawa S, Kuge T, Asayama T. 1990. Migration of bipolar subependymal cells,
precursors of the granule cells of the rat olfactory bulb, with reference to the arrangement of the radial glial fibers. Arch Histol Cytol 53:219 – 226.
Law AKT, Pencea V, Buck CR, Luskin MB. 1999. Neurogenesis and neuronal migration in the neonatal rat forebrain anterior subventricular zone do not require GFAP-positive astrocytes. Dev Biol 216:622– 634.
Laywell ED, Rakic P, Kukekov VG, Holland EC, Steindler DA. 2000. Identification of a multipotent astrocytic stem cell in the immature and adult mouse brain. Proc Natl Acad Sci U S A 25:13883–13888.
Lois C, Alvarez-Buylla A. 1994. Long-distance neuronal migration in the adult mammalian brain. Science 264:1145–1148.
Lois C, Garcia-Verdugo J, Alvarez-Buylla A. 1996. Chain migration of neuronal precursors. Science 271:978 –981.
Luskin MB. 1993. Restricted proliferation and migration of postnatally generated neurons derived from the forebrain subventricular zone. Neuron 11:173–189.
Luzzati F, Peretto P, Aimar P, Ponti G, Fasolo A, Bonfanti L. 2003. Glia-independent chains of neuroblasts through the subcortical parenchyma of the adult rabbit brain. Proc Natl Acad Sci U S A 100:13036 – 13041.
Malatesta P, Hartfuss E, Gotz M. 2000. Isolation of radial glial cells by fluorescent-activated cell sorting reveals a neuronal lineage. Development 127:5253–5263.
Mason HA, Ito S, Corfas G. 2001. Extracellular signals that regulate the tangential migration of olfactory bulb neuronal precursors: inducers, inhibitors, and repellents. J Neurosci 21:7654 – 7663.
Menezes JRL, Dias F, Garson AVB, Lent R. 1998. Restricted distribution of S-phase cells in the anterior subventricular zone of the postnatal mouse forebrain. Anat Embryol 198:205–211.
Menezes JR, Froes MM, Moura Neto V, Lent R. 2000. Gap junctionmediated coupling in the postnatal anterior subventricular zone. Dev Neurosci 22:34 – 43.
Misson JP, Takahashi T, Caviness VS. 1991. Ontogeny of radial and other astroglial cells in murine cerebral cortex. Glia 4:138 –148.
Murase S, Horwitz AF. 2002. Deleted in colorectal carcinoma and differentially expressed integrins mediate the directional migration of neural precursors in the rostral migratory stream. J Neurosci 22:3568 – 3579.
Nadarajah B, Jones AM, Evans WH, Parnavelas JG. 1997. Differential expression of connexins during neocortical development and neuronal circuit formation. J Neurosci 17:3096 –3111
Noctor SC, Flint AC, Weissman TA, Dammerman RS, Kriegstain AR. 2001. Neurons derived from radial glial cells establish radial units in neocortex. Nature 409:714 –720.
Ono K, Tomasiewicz H, Magnuson T, Rutishauser U. 1994. N-Cam mutation inhibits tangential neuronal migration and is phenocopied by enzymatic removal of polysialic acid. Neuron 13:595– 609.
Pencea V, Luskin MB. 2003. Prenatal development of the rodent rostral migratory stream. J Comp Neurol 463:402– 418.
Peretto P, Merighi A, Fasolo A, Bonfanti L. 1997. Glial tubes in the rostral migratory stream of the adult rat. Brain Res Bull 42:9 –21.

Peretto P, Merighi A, Fasolo A, Bonfanti L. 1999. The subependymal layer in rodents: a site of structural plasticity and cell migration in the adult mammalian brain. Brain Res Bull 49:221–243.

Peretto P, Dati C, De Marchis S, Kim HK, Ukhanova M, Fasolo A, Margolis FL. 2004. Expression of the secreted factors noggin and bone morphogenetic proteins in the subependymal layer and olfactory bulb of the adult mouse brain. Neuroscience 128:685– 696.

Pixley SKR, De Vellis J. 1984. Transition between immature radial glia and mature astrocytes studied with a monoclonal antibody to vimentin. Dev Brain Res 15:201–209.

Rakic P. 2003. Developmental and evolutionary adaptations of cortical radial glia. Cereb Cortex 13:541–549.

Rougon G, Dubois C, Buckley N, Magnani JL, Zollinger W. 1986. A monoclonal antibody against meningococcus group B polysacharides distinguishes embryonic from adult N-CAM. J Cell Biol 103:2429 –2437.

Rousselot P, Lois C, Alvarez-Buylla A. 1995. Embryonic (psa) N-CAM reveals chains of migrating neuroblasts between the lateral ventricle and the olfactory bulb of adult mice. J Comp Neurol 351:51– 61.

Shaw G, Osborn M, Weber K. 1981. An immunofluorescence microscopical study of the neurofilament triplet proteins, vimentin and glial fibrillary acidic protein within the adult rat brain. Eur J Cell Biol 26:68 – 82.

Shu T, Butz KG, PlachezC, Gronostajski RM, Linda J, Richards LJ. 2003 Abnormal development of forebrain midline glia and commissural projections in Nfia knock-out mice. J Neurosci 23:203–212.

Smart I. 1961. The subependymal layer of the mouse brain and its cell production as shown by radioautography after thymidine-H3 injection. J Comp Neurol 116:325–338.

Staugaitis SM, Zerlin M, Hawkes R, Levine JM, Goldman JE. 2001. Aldolase C/Zebrin II expression in the neonatal rat forebrain reveals cellular heterogeneity within the subventricular zone and early astrocyte differentiation. J Neurosci 21:6195– 6205.

Steindler DA, Kukekov VG, Brannon Thomas L, Fillmore H, Suslov O, Scheffler B, O'Brien T, Kusakabe M, Laywell ED. 1998. Boundary molecules during brain development, injury, and persistent neurogenesis. Prog Brain Res 117:179 –196.

Steiner B, Kronenberg G, Jessberger S, Brandt MD, Reuter K, Kempermann G. 2004. Differential regulation of gliogenesis in the context of adult hippocampal neurogenesis in mice. Glia 46:41–52.

Theis M, Sohl G, Speidel D, Kuhn R, Willecke K. 2003. Connexin43 is not expressed in principal cells of mouse cortex and hippocampus. Eur J Neurosci 18:267–274.

Tramontin AD, Garcia-Verdugo JM, Lim DA, Alvarez-Buylla A. 2003. Postnatal development of radial glia and the ventricular zone (VZ): a continuum of the neural stem cell compartment. Cereb Cortex 13:580 – 587.

Wichterle H, Garcia-Verdugo JM, Alvarez-Buylla A. 1997. Direct evidence for homotypic, glia-independent neuronal migration. Neuron 18:779 – 791.

Yamamoto T, Ochalski A, Hertzberg EL, Nagy JI. 1990. On the organization of astrocytic gap junctions in rat brain as suggested by LM and EM immunohistochemistry of connexin43 expression. J Comp Neurol 302: 853– 883.

Yang P, Yin X, Rutishauser U. 1992. Intercellular space is affected by the polysialic acid content of N-CAM. J Cell Biol 116:1487–1496.